

Macrocyclic Transition-Metal Parashift Complexes for MRI at Clinical and Pre-clinical Magnetic Fields

Nicola J. Rogers,^{*a} Chowan Ashok Kumar,^a Carlson Alexander,^a Daniel Bowdery,^b Galina Pavlovskaya,^c and Peter Harvey.^{c,d}

^a Department of Chemistry, Hong Kong Baptist University, Kowloon Tong, Hong Kong.

^b Department of Chemistry, University of Warwick, Coventry CV4 7AL, UK.

^c Sir Peter Mansfield Imaging Centre, School of Medicine, University of Nottingham, University Park, Nottingham NG7 2RD, UK.

^d School of Chemistry, University of Nottingham, University Park, Nottingham NG7 2RD, UK.

Supplementary Information

Contents

1. General Experimental Details.....	1
2. Experimental Section.....	3
3. Experimental Data for Compounds Synthesised.....	11
4. Fitting Field-dependent Proton Relaxation Data.....	59
5. Phantom Imaging Experiments.....	62

1. General Experimental Details

1.1. Reagents and solvents

Methanol (99.9%, HPLC grade), (International Laboratory USA); acetone (lab grade, UN1000, Class 3, PGII), dichloromethane (AR) (Standard chemical, STC); acetonitrile (HPLC grade) (RCI Labscan); 2-(Bromomethyl)-6-methylpyridine (97%), methanesulfonic anhydride (98%), cyclen (97%), 1,4,7-triazacyclononane (TACN, 98%), Iron(II) chloride tetrahydrate (99.95% metal basis), Cobalt(II) chloride hexahydrate (99.7%) (Macklin); deuterium oxide (99.9% atom % D) (Sigma-Aldrich); Manganese chloride tetrahydrate ($\geq 99\%$), Nickel chloride hexahydrate (97%) (Aladdin chemicals); zinc perchlorate hexahydrate (Reagent grade) (Thermo scientific); potassium carbonate, Copper(II) chloride dihydrate (AR), Cobaltous nitrate hexahydrate (AR) (Dieckmann chemicals); Chloroform (D, 99.8% + 0.03% v/v TMS + silver foil) (Cambridge isotope laboratories, Inc.); nitric acid (>68%, PrimarPlus, trace analysis grade) (Fisher scientific). Deionized water was used throughout. 5-*tert*-butylpyridin-2-yl)methanol was synthesized using 5-bromo-2-methyl-pyridine (98%) (Fluorochem), *tert*-butylmagnesium chloride solution (2.0 M) in diethyl ether, CuCN (>98%), 3-chloroperbenzoic acid (77%), trifluoroacetic anhydride (synthesis grade), absolute ethanol (lab grade) (Sigma-Aldrich).

1.2. Vacuum processing, TLC, flash and column chromatography

A Heidolph Laborota 4000-efficient rotary evaporator was used to evaporate solvents under reduced pressure and compounds were dried using a Schlenk line with a Titan RV3 Vacuum Pump. Filtrations were performed under gravity using a Whatman filter paper (grade 1 circles) on a glass funnel or using celite (Aladdin Chemicals) under vacuum. Column chromatography was performed using silica gel (100-200M mesh, Aladdin) or neutral alumina (200-300 mesh, pH = 7.5 ± 0.5 , Dieckmann). Analytical thin layer chromatography (TLC) was performed on aluminum sheet supported silica gel plates coated with silica gel 60 F₂₅₄ (0.2 mm, Merck) or aluminum sheet supported neutral Aluminium oxide 60 F₂₅₄ (Merck) using different solvent systems as mobile phase. The compounds were visualized for TLC by iodine or potassium permanganate stain, and under UV light. Melting points for organic compounds were recorded using Cole-Parmer[®] MP-250 series digital melting point apparatus.

1.3. NMR Spectroscopy

NMR data were collected using the following instruments; 60 MHz (1.4 T) benchtop Magritek NMR at (Temp=299 K), 80 MHz (1.9 T) Bruker benchtop NMR (Temp = 300 K), 300 MHz Bruker NMR (Temp = 296 \pm 1 K), 400 MHz Bruker NMR (Temp = 296 \pm 1 K), 500 MHz Bruker NMR (Temp = 298 K), 600 MHz Bruker NMR (Temp=295 K), and 700 MHz Bruker NMR (Temp = 298 K). Samples were dissolved at 5-10 mg mL⁻¹ concentration in D₂O, in standard 5 mm NMR tubes. ¹H and ¹³C resonances of diamagnetic ligands and Zn(II) complexes were assigned using *J* coupling values, HMBC and HSQC NMR. Paramagnetic NMR spectra were measured using large sweepwidths (e.g. SW=400 ppm), short acquisition and delay times (e.g. aq=0.1 s, d1 = 0.1 s), and a large number of scans (e.g. ns=512). Spectra were processed using line broadening of 5-25 Hz. *T*₁ measurements were performed using an inversion recovery sequence with 10 variable delay times, setting the maximum delay time to 5 × *T*₁. Three independent measurements were performed, and the mean is quoted.

1.4. Mass Spectrometry

Low resolution mass spectrometry was performed using an Agilent 6130B single Quad ESI or a SCIEX 3500 Triple Quad spectrometer. High-resolution mass spectrometry was performed using a SCIEX 6600 Triple TOF spectrometer or a Bruker Compact Q-TOF, or a Bruker Daltonics Autoflex maX LRF MALDI-TOF MS system.

1.5. UV-Vis Photoabsorption Spectroscopy

UV-Vis absorption spectra were measured using an Agilent Cary 8454 Spectrophotometer. Sample solutions were measured using standard 1 cm pathlength quartz cuvettes.

1.6. Crystallography

Crystallography data was collected using either a Rigaku Oxford Diffraction Synergy-S diffractometer with a dual source equipped with a Hybrid pixel array detector or using using $K\alpha$ radiation ($\lambda = 0.71073 \text{ \AA}$) on a Bruker D8V Venture (Photon II 14 detector, $I\mu\text{S}$ 3.0 microfocus sealed tube sources (Cu and Mo) diffractometer) equipped with a Cobra low temperature device. The crystal was kept at 302 K or 100 K during data collection. Using Olex2,¹ the structure was solved with the ShelXS² structure solution program using Direct Methods and refined with the ShelXL³ refinement package using Least Squares minimisation. All non-hydrogen atoms were refined anisotropically; hydrogen atoms were placed in the calculated positions and refined in riding mode. X-ray crystal structure images were produced using Mercury CSD 3.6 software using data from the Cambridge Structural Database.

1.7. Bulk Magnetic Susceptibility Measurements

Bulk magnetic susceptibilities (BMS) were measured using the Evans method at $297 \pm 1 \text{ K}$,^{4,5} which originates from the partial alignment of the magnetic moments of paramagnetic species by the magnetic field, affecting the entire sample. A D_2O (5% v/v *tert*-butyl alcohol) solution of the complex (ca 1-10 mM) was placed in a 5 mm NMR tube, containing a diamagnetic sample reference of D_2O (5% v/v *tert*-butyl alcohol) within a coaxial insert tube. The BMS was determined from the frequency shift of the *tert*-butyl signal of *tert*-butyl alcohol, with respect to the diamagnetic sample.

The effective magnetic susceptibilities were calculated from the frequency shift as follows:

$$\Delta\delta = \frac{4\pi cs}{T} \left(\frac{\mu_{\text{eff}}}{2.84} \right)^2 \times 10^3$$

Where c is the concentration of the paramagnetic solute in mol dm^{-3} , s is dependent of the shape of the sample and its position in the magnetic field ($s = 1/3$ for a cylinder within a superconducting magnet), T is the absolute temperature (in K), and μ_{eff} is the effective magnetic susceptibility.

¹ Dolomanov, O.V., Bourhis, L.J., Gildea, R.J., Howard, J.A.K. & Puschmann, H. (2009), *J. Appl. Cryst.* **42**, 339-341.

² Sheldrick, G.M. (2008). *Acta Cryst.* **A64**, 112-122.

³ Sheldrick, G.M. (2015). *Acta Cryst.* **C71**, 3-8

⁴ S. C. Chu, Y. Xu, J. A. Balschi and C. S. Springer, Jr., *Magn Reson Med*, 1990, **13**, 239-262.

⁵ D. M. Corsi, C. Platas-Iglesias, H. v. Bekkum and J. A. Peters, *Magnetic Resonance in Chemistry*, 2001, **39**, 723-726.

1.8. Bulk Magnetic Susceptibility Measurements

1.9. MRI

MRI of solution phantoms were performed using at 400 MHz (9.4 T) magnet and a 30 mm ^1H imaging coil (Bruker, Germany).

2. Experimental Section

2.1 Ligand Synthesis

Ligand L^{1a}

The following method was adapted from the literature.¹³ TACN (0.496 g, 3.84 mmol), 2-bromomethyl-6-methyl pyridine (2.26 g, 12.1 mmol, 3.2 eq), and K₂CO₃ (2.6 g, 19 mmol, 4.9 eq) were dissolved in HPLC grade CH₃CN (50 mL) and heated at 70 °C overnight under N₂ (g). The solution was cooled, inorganic solids were removed by filtration, and the solvent was removed under vacuum. The resulting dark red residue was purified by column chromatography on neutral alumina (200-300 mesh, pH = 7.5±0.5, Dieckmann) in 100% CH₂Cl₂ to give the product as an amber oil (1.0 g, 2.2 mmol, 57% yield). *R*_f = 0.41 (10% CH₃OH, CH₂Cl₂, neutral alumina plate). ¹H NMR (400 MHz, CDCl₃, 296 K) δ 7.54 (t, ³*J*_{HH} = 7.5 Hz, 3H, Py-H⁴), 7.35 (d, ³*J*_{HH} = 7.5 Hz, 3H, Py-H^{3/5}), 7.00 (d, ³*J*_{HH} = 7.0 Hz, 3H, Py-H^{3/5}), 3.81 (s, 2H, CH₂Py), 2.89 (s, 12H, CH₂-TACN), 2.53 (s, 9H, CH₃); ¹³C(HSQC) NMR (101 MHz, 296 K, CDCl₃): δ 137.4 (Py-C⁴), 121.5 (Py-C^{3/5}), 120.9 (Py-C^{3/5}), 64.9 (CH₂Py), 56.7 (TACN), 25.2 (CH₃). ESI-MS (+) *m/z* 467.6 [M+Na]⁺.

Ligand L^{2a}

The method below was adapted from the literature.¹³ Cyclen (450 mg, 2.61 mmol), 2-bromomethyl-6-methyl pyridine (2.07 g, 11.1 mmol, 4.3 eq), and K₂CO₃ (1.8 g, 13 mmol, 5.0 eq), were dissolved in HPLC grade CH₃CN (50 mL) and heated at 70 °C overnight under N₂ (g). The solution was cooled, inorganic solids were removed by filtration, and the solvent was removed under vacuum. The resulting dark red residue was purified by column chromatography on neutral alumina (200-300 mesh, pH = 7.5±0.5, Dieckmann) in 100% CH₂Cl₂ to give the product as an amber oil (1.4 g, 2.4 mmol, 90% yield). *R*_f = 0.52 (10% CH₃OH, CH₂Cl₂, neutral alumina plate). ¹H NMR (400 MHz, CDCl₃, 296 K) δ 7.52 (d, ³*J*_{HH} = 8.0 Hz, 4H, Py-H^{3/5}), 7.23 (t, ³*J*_{HH} = 7.5 Hz, 4H, Py-H⁴), 6.89 (d, ³*J*_{HH} = 8.0 Hz, 4H, Py-H^{3/5}), 3.57 (s, 8H, CH₂Py), 2.72 (s, 16H, cyclen) 2.41 (s, 12H, CH₃); ¹³C(HSQC) NMR (101 MHz, 296 K, CDCl₃): δ 137.3 (Py-C^{3/5}), 137.1 (Py-C⁴), 121.8 (Py-C^{3/5}), 61.3 (CH₂Py), 53.2 (cyclen), 24.6 (CH₃). ESI-MS (+) *m/z* 593.0 [M+H]⁺.

Ligand L^{1b}

(5-tert-Butylpyridin-2-yl)methyl methanesulfonate (372 mg, 1.53 mmol) was synthesised from (5-tert-butylpyridin-2-yl)methanol (318 mg, 1.93 mmol) as previously described,⁵ and used immediately without further purification. The mesylate (3 eq) was dissolved in CH₃CN (3 mL) under nitrogen and 1,4,7-triazacyclonone (65 mg, 0.50 mmol, 1 eq) and K₂CO₃ (211 mg, 1.52 mmol, 3 eq) were added. The reaction mixture was stirred at 60 °C under nitrogen for 14 h. The resultant precipitate was separated by centrifugation, and the solid washed with H₂O (3 × 5 mL). The solvent was removed under reduced pressure to give a pale-yellow solid (117 mg, 0.21 mmol, 40 % yield) which was used without further purification. ¹H NMR (400 MHz, CDCl₃, 296 K) δ 8.54 (d, ⁴*J*_{HH} = 2.0 Hz, 3H, Py-H⁶), 7.64 (dd, ³*J*_{HH} = 8.0 Hz, ⁴*J*_{HH} = 2.0 Hz, 3H, Py-H⁴), 7.42 (d, ³*J*_{HH} = 8.0 Hz, 3H, Py-H³), 3.79 (s, 6H, CH₂Py), 2.88 (s, 12H, CH₂-TACN), 1.34 (s, 27H, CH₃); ¹³C{¹H} NMR (101 MHz, 296 K, CDCl₃): δ 157.5 (Py-C²), 146.4 (Py-C⁶), 144.1 (Py-C⁵), 133.5 (Py-C⁴), 122.6 (Py-C³), 64.5 (CH₂Py), 55.9 (TACN), 33.5 (C(CH₃)₃), 31.7 (CH₃). ESI-MS (+) *m/z*

571.9 [M+H]⁺. HR MALDI-TOF: [C₃₆H₅₄N₆]⁺ calcd. = 571.4488, found = 571.4490. m.p. = 113-114 °C.

Ligand L^{2b}

(5-tert-Butylpyridin-2-yl)methyl methanesulfonate was synthesised from (5-tert-Butylpyridin-2-yl)methanol, as previously described,⁵ and used immediately. (5-tert-butylpyridin-2-yl)methyl methanesulfonate (264.4 mg, 1.09 mmol) was added to a mixture of anhydrous CH₃CN (20 mL), K₂CO₃ (978 mg) and cyclen (50.8 mg). The mixture was heated to 70 °C and stirred under nitrogen for 24 h and then cooled and filtered to removed inorganic salts. The solvent was removed under reduced pressure leaving an orange/brown glassy solid (88.6 mg). This was used without further purification. ¹H NMR (300 MHz, 298 K, CDCl₃) δ 8.39 (s, 4H, H⁶), 7.8-7.2 (8H, H^{3/4}), 3.6-3.0 (24H, NCH₂ and cyclen CH₂), 1.21 (s, 36H, C(CH₃)₃). ESI-LRMS (+) m/z 783.6 [M + Na]⁺.

2.2 Metal Complex Synthesis

[ML^{1a}]²⁺, [ML^{2a}]²⁺, [ML^{1b}]²⁺, and [ML^{2b}]²⁺ complexes synthesised from metal chloride salts
The following general method was followed for complexation reactions; Typically, ligand (0.2 mmol, 1 eq) was dissolved in CH₃OH (1 mL), and water (0.5 mL) was added to the solution. To this was added the metal dichloride salt (either FeCl₂·4H₂O, CoCl₂·6H₂O, NiCl₂·6H₂O, CuCl₂·2H₂O, or MnCl₂·4H₂O) (0.27 mmol, 1.2 eq), and the pH was adjusted to pH 7 using NaOH solution (0.1 M). The solution was stirred at room temperature for 2 h and the solvent was removed under vacuum. The residue was dissolved in CH₃OH (0.5 mL) and added dropwise to cold stirring ethyl acetate (20 mL) to give a resulting precipitate that was isolated by vacuum filtration.

[FeL^{1a}]Cl₂

The resulting pale-yellow precipitate was isolated by filtration to give the product as a pale orange/yellow powder (90 mg, 51% yield), as previously reported by Morrow and co-workers.¹³ [note – when dissolved in water the solution is yellow].

¹H NMR (80 MHz, D₂O, 300 K) δ +197 (1H, FWHM=107 Hz, cyclen/arm), +169 (1H, FWHM=132 Hz, cyclen/arm), +99 (1H, FWHM=122 Hz, cyclen/arm), +73 (1H, FWHM=148 Hz, cyclen/arm), +53 (1H, FWHM=58 Hz, Py-H⁵), +34 (1H, FWHM=42 Hz, Py-H³), +22 (3H, FWHM=152 Hz, CH₃), -4 (1H, FWHM=50 Hz, Py-H⁴), -12 (1H, FWHM=199 Hz, cyclen/arm), -20 (1H, FWHM=183 Hz, cyclen/arm). *T*₁ (δ = 22 ppm, CH₃) = 3.374, ms, SD = 2.692E-2. (*R*₁ = 295 Hz, *R*₂ = 480 Hz). ESI-MS (+) *m/z* 250.0 [M]²⁺, 535.3 [M+Cl]⁺. *μ*_{eff} = 5.4±0.3 *μ*_B (measured at 296 K, using Evans method, mean±1SD of three measurements). UV-Vis (ε/dm³ mol⁻¹ cm⁻¹, in H₂O): 27500 cm⁻¹ (360 nm, ε=1100), 37000 cm⁻¹ (270 nm, ε=10,000, LC transition), 49000 cm⁻¹ (205 nm, ε=18,000, *sh*, LC transition).

Iron content by ICP-MS = 10.2±3.7 wt.% (expected for [FeL^{1a}]Cl₂ = 9.8 wt.%).

[CoL^{1a}]Cl₂ (expect contains some CoCl₄²⁻ counterions)

The resulting pale blue precipitate was isolated by filtration to give the product as a pale blue/violet powder (69 mg, 55% yield), as previously reported by Morrow and co-workers.¹³ [note – when dissolved in water the solution is pink].

¹H NMR (80 MHz, D₂O, 300 K) δ +201 (1H, FWHM=55 Hz, cyclen/arm), +188 (1H, FWHM=64 Hz, cyclen/arm), +119 (1H, FWHM=57 Hz, cyclen/arm), +65 (1H, FWHM=77 Hz, cyclen/arm), +50 (1H, FWHM=23 Hz, Py-H⁵), +34 (1H, FWHM=25 Hz, Py-H³), +9 (3H, FWHM=65 Hz, CH₃), +6 (1H, FWHM=24 Hz, Py-H⁴), -12 (1H, FWHM=123 Hz, cyclen/arm), -23 (1H, FWHM=110 Hz, cyclen/arm). *T*₁ (δ = +9 ppm, CH₃) = 6.190 ms, SD = 2.692E⁻². (*R*₁ = 160 Hz, *R*₂ = 205 Hz). ESI-MS (+) *m/z* 251.6 [M]²⁺. UV-Vis (H₂O): 9400 cm⁻¹ (1070 nm, *d-d* transition), 18000 cm⁻¹ (550 nm, *sh*, *d-d* transition), 18600 cm⁻¹ (540 nm, *sh*, *d-d* transition), 19500 cm⁻¹ (513 nm, *d-d* transition), 37000 cm⁻¹ (270 nm, LC transition), 49000 cm⁻¹ (205 nm, *sh*, LC transition).

Cobalt content by ICP-MS = 12.4±2.0 wt.% (expected for [CoL^{1a}]Cl₂ = 10.3 wt.%, for [CoL^{2a}](CoCl₄) = 16.7 wt.%, for [CoL^{2a}]₂(CoCl₄)Cl₂ = 13.8%).

[NiL^{1a}]Cl₂ (may contain NiCl₄²⁻ counter ions)

The resulting turquoise/blue precipitate was isolated by filtration to give the product as a pale turquoise/blue powder (100 mg, 76% yield). [note – when dissolved in water solution is pale blue].

¹H NMR (80 MHz, D₂O, 300 K) δ +205 (*br*), +180 (*br*), +125 (*br*), +42 (FWHM=210 Hz, Py-H), +34 (FWHM=175 Hz, Py-H), +13 (FWHM=76 Hz, Py-H⁴), -9 (*br*, CH₃). ESI-MS (+) *m/z* 251.1 [M]²⁺. HR ESI-LCMS: [C₂₇H₃₆N₆Ni]²⁺ calcd. = 251.1172, found = 251.1172. UV-Vis (H₂O): 10700 cm⁻¹ (940 nm, *d-d* transition), 11000 cm⁻¹ (830 nm, *sh*, *d-d* transition), 17000 cm⁻¹ (590 nm, *d-d* transitions), 37000 cm⁻¹ (270 nm, LC transition), 49000 cm⁻¹ (205 nm, *sh*, LC transitions).

Single crystals of C₂₇H₃₆N₆O₈Cl₂Ni were grown from the perchlorate salt following by the slow vapour diffusion of 1,4-dioxane into the compound dissolved in acetonitrile: (*M* = 702.23 g/mol): monoclinic, space group P2₁/c (no. 14), *a* = 14.8189(7) Å, *b* = 11.8401(5) Å, *c* = 33.4481(15) Å, β = 91.670(2)°, *V* = 5866.2(5) Å³, 152269 reflections measured (3.62° ≤ 2θ ≤ 55.044°), 13477 unique (*R* used in all calculations. The final *R* 1 was 0.0883 (*I* > 2σ(*I*)) and *wR* 2, *Z* = 8, *T* = 100.00 K, μ(MoKα) = 0.905 mm⁻¹ = 0.1410, *R* int sigma, *D*calc = 0.0675) which were was 0.1632 (all data).

[CuL^{1a}]Cl₂ (may contain CuCl₄²⁻ counter ions)

The resulting lime green precipitate was isolated by filtration to give the product as a green powder (37 mg, 29% yield). [note – when dissolved in water the solution is turquoise].

¹H NMR (80 MHz, D₂O, 300 K) δ +30 (*br*), +11 (1H, FWHM=150 Hz, Py-H⁴), -5 (*br*, CH₃). ESI-MS (+) *m/z* 253.7 [M]²⁺. HR ESI-LCMS: [C₂₇H₃₆CuN₆]²⁺ calcd. = 253.6143, found = 253.6132. UV-Vis (H₂O): 13500 cm⁻¹ (740 nm, *d-d* transition), 30500 cm⁻¹ (330 nm, *sh*), 37000 cm⁻¹ (270 nm, LC transition), 49000 cm⁻¹ (205 nm, *sh*, LC transition).

Single crystals of C₂₇H₃₆Cl₂CuN₆O₈ were grown by slow anion exchange by adding solid Zn(ClO₄)₂ to an aqueous solution of the chloride salt of the complex [CuL^{1a}]Cl₂. The asymmetric unit contains two copper complexes and four perchlorate counter ions. Crystal structure determination of the crystal data for C₂₇H₃₆N₆O₈Cl₂Cu (*M* = 707.06 g/mol): monoclinic, space group P2₁/c (no. 14), *a* = 15.0287(3) Å, *b* = 11.9831(2) Å, *c* = 33.9757(7) Å, β = 91.6010(10)°, *V* = 6116.3(2) Å³, *Z* = 8, *T* = 300.0 K, μ(MoKα) = 0.948 mm⁻¹, *D*calc = 1.536 g/cm³, 297858

reflections measured ($4.16^\circ \leq 2\Theta \leq 55.78^\circ$), 14604 unique ($R_{\text{int}} = 0.0317$, $R_{\text{sigma}} = 0.0142$) which were used in all calculations. The final R_1 was 0.0443 ($>2\sigma(I)$) and wR_2 was 0.1348 (all data).

[MnL^{1a}]Cl₂

The resulting white precipitate was isolated by filtration to give the product as a white powder (70 mg, 93% yield). [note – when dissolved in water the solution is colourless].

¹H NMR (80 MHz, D₂O, 300 K) broad indiscernible peaks. ESI-MS (+) m/z 249.8 [M]²⁺. HR ESI-LCMS: [C₂₇H₃₆MnN₆]²⁺ calcd. = 249.6186, found = 249.6197. UV-Vis (H₂O): LC transitions 37000 cm⁻¹ (270 nm), 49000 cm⁻¹ (205 nm, *sh*).

[FeL^{1b}]Cl₂

The resulting orange precipitate was isolated by vacuum filtration (21 mg, 0.03 mmol, 60% yield). [note – when dissolved in water solution is orange/yellow].

¹H NMR (400 MHz, 298 K, D₂O) δ 7.80 (d, ³ J_{HH} =8.0 Hz, 3H, Py-H^{3/4}), 7.44 (d, ³ J_{HH} =8.0 Hz, 3H, Py-H^{3/4}), 6.67 (s, 3H, Py-H⁶), 4.05 (d, ² J_{HH} = 17.0 Hz, CH₂-Py), 3.70-3.40 (*br m*, 3H, TACN-H^{ax}), 3.29 (dd, ² J_{HH} =15.5 Hz, ³ J_{HH} =5.5 Hz, 3H, TACN-H^{eq}), 3.07 (dd, ² J_{HH} =12.5 Hz, ³ J_{HH} =5.5 Hz, 3H, TACN-H^{eq}), 2.80-2.40 (*br m*, 3H, CH₂-Py), 2.38 (td, ³ J_{HH} =12.0 Hz, ³ J_{HH} =5.5 Hz, 3H, TACN-H^{ax}), 0.87 (s, 27H, CH₃). ESI-MS (+) m/z 313.8[M]²⁺, 661.9 [M+Cl]⁺. MALDI-TOF HRMS(+): calculated for C₃₆H₅₄ClFeN₆ = 661.3448, found = 661.3468 [M+Cl]⁺.

Single crystals of the FeL^{1b} complex were grown by vapour diffusion of 1,4-dioxane into an acetone solution of [FeL^{1b}]Cl₂. The asymmetric unit contains one iron complex, an [FeCl₃-O-FeCl₃]²⁻ oxide-bridging anion, and a dioxane solvent molecule. Crystal structure determination of the crystal data for 0.5(C₃₆H₅₄FeN₆),0.5(Cl₆Fe₂O),0.5(C₄H₈O₂) (M=1061.81 g/mol): triclinic, space group *P-1* (no. 2), a = 12.4242(10) Å, b = 12.5408(11) Å, c = 16.2487(15) Å, α = 82.332(4)°, β = 76.998(3)°, γ = 83.372(3)°, V = 2435.2(4) Å³, Z = 4, T = 100.00 K, $\mu(\text{MoK}\alpha)$ = 1.253 mm⁻¹, *D*_{calc} = 1.448 g/cm³, 134627 reflections measured ($4.502^\circ \leq 2\Theta \leq 55.066^\circ$), 11143 unique ($R_{\text{int}} = 0.0797$, $R_{\text{sigma}} = 0.0299$) which were used in all calculations. The final R_1 was 0.0424 ($I > 2\sigma(I)$) and wR_2 was 0.1159 (all data).

[CoL^{1b}]Cl₃ (may contain CoCl₄²⁻ counter ions)

The resulting green precipitate was isolated by vacuum filtration. (20 mg, 56 % yield). [note – when dissolved in water the solution is orange].

¹H NMR (400 MHz, 298 K, D₂O) δ 7.93 (*br d*, 3H, Py-H^{3/4}), 7.43 (*br d*, 3H, Py-H^{3/4}), 5.65 (s, 3H, Py-H⁶), 4.38 (*br d*, 3H, CH₂Py), 4.27 (*br d*, 3H, CH₂Py), 3.89 (*br t*, 3H, TACN-H^{ax}), 3.46 (*br d*, 3H, TACN-H^{eq}), 2.81 (*br d*, 3H, TACN-H^{eq}), 2.65 (*br t*, 3H, TACN-H^{ax}), 0.45 (s, 27H, CH₃). ¹³C NMR (101 MHz, 296 K, D₂O): δ_{C} 161.5 (Py-C^{2/5}), 152.4 (Py-C^{2/5}), 144.6 (Py-C⁶), 141.6 (Py-C^{3/4}), 125.5 (Py-C^{3/4}), 68.2 (CH₂Py), 65.1 (TACN-C'), 62.4 (TACN-C''), 33.4 (C(CH₃)₃), 29.0 (CH₃). ESI-MS (+) m/z 210.4 [M]³⁺, 315.3 [M]²⁺, 663.9 [M+Cl]⁺. MALDI-TOF HRMS(+): calculated for C₃₆H₅₄ClCoN₆ = 664.3430, found 664.3451 [M+Cl]⁺. UV-Vis (H₂O): 21000 cm⁻¹ (473 nm, *d-d* transition), 28000 cm⁻¹ (347 nm, *sh*), 33000 cm⁻¹ (303 nm, *sh*), 40000 cm⁻¹ (245 nm, LC transition), 47000 cm⁻¹ (212 nm, LC transition).

The perchlorate salt of $[\text{CoL}^{\text{1b}}]^{3+}$ was formed by slow anion exchange, by adding solid $\text{Zn}(\text{ClO}_4)_2$ to an aqueous solution of the chloride/tetrachlorocobaltate(II) salt of the complex. Single crystals of $\text{C}_{36}\text{H}_{54}\text{C}_{13}\text{CoN}_6\text{O}_{12}$ were grown from the perchlorate salt by the slow vapour diffusion of ethyl acetate into a methanol solution of $[\text{CoL}^{\text{1b}}](\text{ClO}_4)_3$. The asymmetric unit contains one Cobalt complex and three perchlorate anions. Crystal structure determination of the crystal data for $\text{C}_{36}\text{H}_{54}\text{C}_{13}\text{CoN}_6\text{O}_{12}$ ($M = 928.13$ g/mol): orthorhombic, space group Pbca (no. 61), $a = 15.697(2)$ Å, $b = 16.444(2)$ Å, $c = 32.890(4)$ Å, $V = 8489.8(19)$ Å³, $Z = 8$, $T = 100.00$ K, $\mu(\text{MoK}\alpha) = 0.660$ mm⁻¹, $D_{\text{calc}} = 1.452$ g/cm³, 436847 reflections measured ($4.36^\circ \leq 2\theta \leq 54.964^\circ$), 9734 unique ($R_{\text{int}} = 0.0764$, $R_{\text{sigma}} = 0.0194$) which were used in all calculations. The final R_1 was 0.0717 ($I > 2\sigma(I)$) and wR_2 was 0.2089 (all data).

$[\text{FeL}^{\text{2a}}]\text{Cl}_2$

The resulting pale-yellow precipitate was isolated by filtration to give the product as a pale-yellow powder (107 mg, 78% yield) as previously reported by Morrow and co-workers.¹³ [note – when dissolved in water the solution is orange/yellow].

¹H NMR (80 MHz, D₂O, 300 K) δ +278 (br), +194 (br), +186 (br), +132 (1H, FWHM=115 Hz), +93 (br), +65 (1H, FWHM=225 Hz), +63 (1H, FWHM=120 Hz), +56 (1H, FWHM=62 Hz), +11 (1H, FWHM=46 Hz), +8 (1H, FWHM=40 Hz), -27 (br), -31 (br), -57 (3H, FWHM=270 Hz, CH₃), -78 (br). T_1 ($\delta = -57$ ppm, CH₃) = 1.257 ms, SD = 0.0105 ($R_1 = 796$ Hz, $R_2^* = 880$ Hz). ESI-MS (+) m/z 324.0 $[\text{M}]^{2+}$ $\mu_{\text{eff}} = 5.8 \pm 0.7 \mu_B$ (measured at 296 K, using Evans method, mean \pm 1 SD of three measurements). UV-Vis ($\epsilon/\text{dm}^3 \text{ mol}^{-1} \text{ cm}^{-1}$, in H₂O): 28000 cm⁻¹ (355 nm, $\epsilon=1100$, *sh*), 37000 cm⁻¹ (270 nm, $\epsilon=13,000$, LC transition), 37500 cm⁻¹ (265 nm, $\epsilon=15,000$, LC transition), 48500 cm⁻¹ (205 nm, $\epsilon=22,000$, *sh*, LC transition).

Iron content by ICP-MS = 7.9 ± 0.9 wt.% (expected for $[\text{FeL}^{\text{2a}}]\text{Cl}_2 = 7.8$ wt.%).

$[\text{CoL}^{\text{2a}}]\text{Cl}_2$ (expect contains some CoCl_4^{2-} counter ions)

The resulting pale-blue precipitate was isolated by filtration to give the product as a pale blue powder (40 mg, 0.055 mmol, 54% yield), as previously reported by Morrow and co-workers.¹³ [note – when dissolved in water solution the is pale orange/pink]

¹H NMR (80 MHz, D₂O, 300 K) δ +205 (br), +134 (FWHM=240 Hz), +95 (br), +77 (br), +56 (1H, FWHM=190 Hz), +25 (1H, FWHM=170 Hz), +11 (1H, FWHM=80 Hz), -80 (br), -122 (br, CH₃). ESI-MS (+) m/z 325.7 $(\text{M})^{2+}$. UV-Vis (H₂O): 11500 cm⁻¹ (875 nm, *d-d* transition), 19000 cm⁻¹ (525 nm, *d-d* transition), 21500 cm⁻¹ (460 nm, *sh*), 37000 cm⁻¹ (270 nm, $\epsilon=12,000$, LC transition), 37500 cm⁻¹ (265 nm), 48500 cm⁻¹ (205 nm, *sh*, LC transition).

Cobalt content by ICP-MS = 10.0 ± 1.0 wt.% (expected for $[\text{CoL}^{\text{2a}}]\text{Cl}_2 = 8.2$ wt.%, for $[\text{CoL}^{\text{2a}}](\text{CoCl}_4) = 13.8$ wt.%, for $[\text{CoL}^{\text{2a}}]_2(\text{CoCl}_4)\text{Cl}_2 = 11.2\%$).

$[\text{NiL}^{\text{2a}}]\text{Cl}_2$ (may contain NiCl_4^{2-} counter ions)

The resulting turquoise precipitate was isolated by filtration to give the product as a dark turquoise solid (77 mg, 61% yield). [note – when dissolved in water the solution is orange].

¹H NMR (80 MHz, D₂O, 300 K) δ +235 (br), -185 (br), +135 (br) +115 (br), +65 (1H, FWHM=115 Hz), +40 (br), +21 (1H, FWHM=95 Hz, *py-H*), +16 (1H, FWHM=160 Hz), +12 (1H, FWHM=90 Hz, *Py-H*), +8 (3H, CH₃), +1 (3H, CH₃), -25 (br). ESI-MS (+) m/z 324.7 $[\text{M}]^{2+}$ HR ESI-LCMS:

$[\text{C}_{36}\text{H}_{48}\text{N}_8\text{Ni}]^{2+}$ calcd. = 325.1672, found = 325.1677. UV-Vis (H_2O): 10000 cm^{-1} (1000 nm, *d-d* transition), 11500 cm^{-1} (870 nm, *d-d* transition), 13000 cm^{-1} (7700 nm, *br*, *d-d* transition), 19000 cm^{-1} (530 nm, *d-d* transition), 21000 cm^{-1} (475 nm, *d-d* transition), 25000 cm^{-1} (405 nm), 37000 (270 nm, LC transition), 49000 cm^{-1} (205 nm, *sh*, LC transition).

$[\text{CuL}^{2a}]\text{Cl}_2$ (may contain CuCl_4^{2-} counter ions)

The resulting green precipitate was isolated by filtration to give the product as an emerald powder (99 mg, 70% yield). [note – when dissolved in water the solution is turquoise].

^1H NMR (80 MHz, D_2O , 300 K) broad, non-discernible peaks spanning +20 to -5 ppm. ESI-MS (+) m/z 327.4 $[\text{M}]^{2+}$. HR ESI-LCMS: $[\text{C}_{36}\text{H}_{48}\text{CuN}_8]^{2+}$ calcd. = 327.6644, found = 327.6653. UV-Vis (H_2O): 9800 cm^{-1} (1020 nm, *d-d* transition), 14600 cm^{-1} (685 nm, *d-d* transition), 30500 cm^{-1} (330 nm, *sh*), 37000 cm^{-1} (270 nm, LC transition), 37500 cm^{-1} (265 nm, LC transition), 49000 cm^{-1} (205 nm, *sh*, LC transition).

Single crystals of $\text{C}_{27}\text{H}_{50}\text{Cl}_4\text{CuN}_8\text{O}_{17}$ were grown by slow anion exchange by adding solid $\text{Zn}(\text{ClO}_4)_2$ to an aqueous solution of the chloride salt of the complex $[\text{CuL}^{2a}]\text{Cl}_2$. The asymmetric unit contains a five-coordinate copper complex with two coordinated pyridine arms and two protonated pyridyl units, with four perchlorate counter ions and two methanol solvent molecules. Crystal structure determination of the crystal data for $\text{C}_{36}\text{H}_{50}\text{Cl}_4\text{CuN}_8\text{O}_{17}$ ($M = 1072.18$ g/mol): triclinic, space group P-1 (no. 2), $a = 11.4580(2)$ Å, $b = 12.5503(2)$ Å, $c = 16.0052(2)$ Å, $\alpha = 85.0880(10)^\circ$, $\beta = 83.0030(10)^\circ$, $\gamma = 76.6270(10)^\circ$, $V = 2218.55(6)$ Å³, $Z = 2$, $T = 100.15$ K, $\mu(\text{CuK}\alpha) = 3.629$ mm⁻¹, $D_{\text{calc}} = 1.605$ g/cm³, 29200 reflections measured ($5.58^\circ \leq 2\theta \leq 134.08^\circ$), 7903 unique ($R_{\text{int}} = 0.0352$, $R_{\text{sigma}} = 0.0312$) which were used in all calculations. The final R_1 was 0.0413 ($>2\sigma(I)$) and wR_2 was 0.1117 (all data).

$[\text{CoL}^{2b}]\text{Cl}_2$ (may contain CoCl_4^{2-} counter ions)

The resulting blue/green solid was isolated by filtration (48.5 mg, 58%). ^1H NMR (500 MHz, 298 K, 25 D_2O) δ -1 ppm (s, 36H, $\text{C}(\text{CH}_3)_3$). ESI-MS (+) m/z 409.8 $[\text{M}]^{2+}$. ESI-HRMS (+) calculated for $[\text{CoC}_{48}\text{H}_{72}\text{N}_8]^{2+}$ 409.7600, found 409.7597. UV-Vis (H_2O): 17600 cm^{-1} (565 nm, *d-d* transition), 19200 cm^{-1} (520 nm, *d-d* transition), 20700 cm^{-1} (480 nm, *d-d* transition), 37500 cm^{-1} (265 nm, LC transition), 48000 cm^{-1} (210 nm, *sh*, LC transition).

Single crystals of $\text{C}_{49}\text{H}_{72}\text{Cl}_4\text{Co}_2\text{N}_8\text{O}$ were grown in $\text{CH}_3\text{OH}/\text{Et}_2\text{O}$. The asymmetric unit contains a cobalt complex, a CoCl_4^{2-} counter ion, a disordered molecule of methanol, and two of the pyridines lie further out of the coordination sphere of the cobalt. Crystal structure determination of the crystal data for $\text{C}_{49}\text{H}_{72}\text{Cl}_4\text{Co}_2\text{N}_8\text{O}$ ($M = 1048.80$ g/mol): monoclinic, space group $\text{P}2_1/\text{n}$ (no. 14), $a = 10.70786(8)$ Å, $b = 31.0143(3)$ Å, $c = 16.12782(14)$ Å, $\beta = 101.6184(8)^\circ$, $V = 5246.25(8)$ Å³, $Z = 4$, $T = 100(2)$ K, $\mu(\text{Cu K}\alpha) = 7.159$ mm⁻¹, $D_{\text{calc}} = 1.328$ g/cm³, 132377 reflections measured ($5.7^\circ \leq 2\theta \leq 160.522^\circ$), 11380 unique ($R_{\text{int}} = 0.0877$, $R_{\text{sigma}} = 0.0323$) which were used in all calculations. The final R_1 was 0.0505 ($I > 2\sigma(I)$) and wR_2 was 0.1496 (all data).

$[\text{ZnL}^{1a}](\text{ClO}_4)_2$

Ligand L^{1a} (50.0 mg, 0.112 mmol) was dissolved in CH_3CN (1 mL, HPLC grade), and $\text{Zn}(\text{ClO}_4)_2 \cdot 6\text{H}_2\text{O}$ (53.0 mg, 0.142, 1.3 eq.) was added. The solution was stirred at room temperature for 2 h, and ethyl acetate (10 mL) was added to the stirring solution, inducing precipitation. The

cream precipitate was collected by centrifugation, to give a pale-yellow solid (66 mg, 0.093 mmol, 83 % yield.)

^1H NMR (400 MHz, 296 K, CD_3CN) δ 8.02 (t, $^3J_{\text{HH}}=8.0$ Hz, 3H, PyH^4), 7.47 (2 \times d, $^3J_{\text{HH}}=8.0$ Hz, 6H, PyH^3 , PyH^5), 4.23 (d, $^2J_{\text{HH}}=15.0$ Hz, 3H, CH_2Py), 3.79 (d, $^2J_{\text{HH}}=15.0$ Hz, 3H, CH_2Py), 3.23 (m, 3H, TACN- H^{ax}), 2.92 (dd, $^2J_{\text{HH}}=15.0$ Hz, $^3J_{\text{HH}}=5.0$ Hz, 3H, TACN- H^{eq}), 2.84 (dd, $^2J_{\text{HH}}=13.0$ Hz, $^3J_{\text{HH}}=5.0$ Hz, 3H, TACN- H^{eq}), 2.17 (s, 9H, CH_3), 1.80 (td, $^2J_{\text{HH}}=13$ Hz, $^3J_{\text{HHax}}=13$ Hz, $^3J_{\text{HHeq}}=5$ Hz, 3H, TACN- H^{ax}). $^{13}\text{C}\{^1\text{H}\}$ NMR (101 MHz, 296 K, CD_3CN) δ 160.8 (Py- $\underline{\text{C}}(\text{CH}_3)$), 156.2 (Py C^2), 142.5 (Py C^4), 129.0 (Py C^5), 124.2 (Py C^3), 64.3 (CH_2Py), 55.7 (TACN- C'), 52.5 (TACN- C''), 24.4 (CH_3). ESI-MS (+) m/z [M] $^{2+}$ 254.4. HR ESI-LCMS: [$\text{C}_{27}\text{H}_{36}\text{N}_6\text{Zn}$] $^{2+}$ calcd. = 251.1141, found = 254.1130. UV-Vis ($\epsilon/\text{dm}^3 \text{ mol}^{-1} \text{ cm}^{-1}$, in 0.5% CH_3CN , H_2O): LC transitions 37000 cm^{-1} (270 nm, $\epsilon=12,000$), 49000 cm^{-1} (205 nm, $\epsilon=19,000$, *sh*).

Single crystals of $\text{C}_{27}\text{H}_{36}\text{Cl}_2\text{ZnN}_6\text{O}_8$ were grown from slow evaporation of acetonitrile from a solution of [$\text{ZnL}^{1\text{a}}$](ClO_4) $_2$. The asymmetric unit contains two zinc complexes and four perchlorate counters ions. Crystal Data for $\text{C}_{27}\text{H}_{36}\text{Cl}_2\text{ZnN}_6\text{O}_8$ (M =708.89 g/mol): monoclinic, space group $\text{P2}_1/\text{c}$ (no. 14), $a = 15.0523(3)$ Å, $b = 12.0637(2)$ Å, $c = 33.9291(6)$ Å, $\beta = 91.4400(10)^\circ$, $V = 6159.12(19)$ Å 3 , $Z = 8$, $T = 302.0$ K, $\mu(\text{MoK}\alpha) = 1.030$ mm $^{-1}$, $D_{\text{calc}} = 1.529$ g/cm 3 , 279151 reflections measured ($4.32^\circ \leq 2\theta \leq 54.96^\circ$), 14100 unique ($R_{\text{int}} = 0.0309$, $R_{\text{sigma}} = 0.0135$) which were used in all calculations. The final R_1 was 0.0453 ($>2\text{sigma}(I)$) and wR_2 was 0.1409 (all data).

[$\text{ZnL}^{2\text{a}}$](ClO_4) $_2$

Ligand $\text{L}^{2\text{a}}$ (91.8 mg, 0.155 mmol) was dissolved in CH_3CN (1 mL, HPLC grade), and $\text{Zn}(\text{ClO}_4)_2 \cdot 6\text{H}_2\text{O}$ (69.0 mg, 0.186, 1.2 eq.) was added. The solution was stirred at room temperature for 2 h, and ethyl acetate (10 mL) was added to the stirring solution, inducing precipitation. The cream precipitate was collected by centrifugation, to give a pale-yellow solid (88 mg, 0.103 mmol, 66 % yield.)

^1H NMR (80 MHz, 300 K, CD_3CN) δ 8.04 (t, $^3J_{\text{HH}}=7.5$ Hz, 4H, PyH^4), 7.44 (2 \times d, $^3J_{\text{HH}}=7.5$ Hz, 8H, PyH^3 , PyH^5), 4.49-3.55 (m, 8H, CH_2Py), 3.30-2.89 (m, 16H, cyclen- CH_2) 2.17 (s (*br*), 12H, CH_3). ESI-MS(+) m/z [M] $^{2+}$ 328.3, [$\text{M}+\text{ClO}_4$] $^+$ 755.5. HR ESI-LCMS: [$\text{C}_{36}\text{H}_{48}\text{N}_8\text{Zn}$] $^{2+}$ calcd. = 328.1641, found = 328.1661. UV-Vis ($\epsilon/\text{dm}^3 \text{ mol}^{-1} \text{ cm}^{-1}$, in 0.5% CH_3CN , H_2O): LC transitions 375000 cm^{-1} (270 nm, $\epsilon=17,000$), 49000 cm^{-1} (205 nm, $\epsilon=21,000$, *sh*).

[$\text{CoL}^{2\text{a}}$](NO_3) $_2$

Ligand $\text{L}^{2\text{a}}$ (106 mg, 0.18 mmol) was dissolved in CH_3CN (2 mL) and $\text{Co}(\text{NO}_3)_2 \cdot 6\text{H}_2\text{O}$ (63 mg, 0.22 mmol, 1.2 eq.) was added to the solution, which was stirred for 2 h at room temperature. Cold ethyl acetate (50 mL) was added, to give a pink precipitate, which was collected by vacuum filtration, and washed further with ethyl acetate (3 \times 10 mL) and dried under suction to give the title product as a pink solution (87 mg, 60 % yield). ^1H NMR (80 MHz, D_2O , 300 K) δ +204 (br), +13 (FWHM=230 Hz), +95 (br), +76 (br), +57 (1H, FWHM=200 Hz), +25 (1H, FWHM=150 Hz), +12 (1H, FWHM=55 Hz), -80 (br), -122 (br, CH_3). ESI-MS (+) m/z (M) $^{2+}$, 713.4 ($\text{M}+\text{NO}_3$) $^+$ $\mu_{\text{eff}} = 5.1 \pm 0.3 \mu_B$ (measured at 296 K, using Evans method, mean \pm 1SD of three measurements). Cobalt content by ICP-MS = 6.9 \pm 0.7 wt.% (expected for [$\text{CoL}^{2\text{a}}$](NO_3) $_2$ = 7.6 wt.%).

3. Experimental Data for Compounds Synthesised Ligand L^{1a}

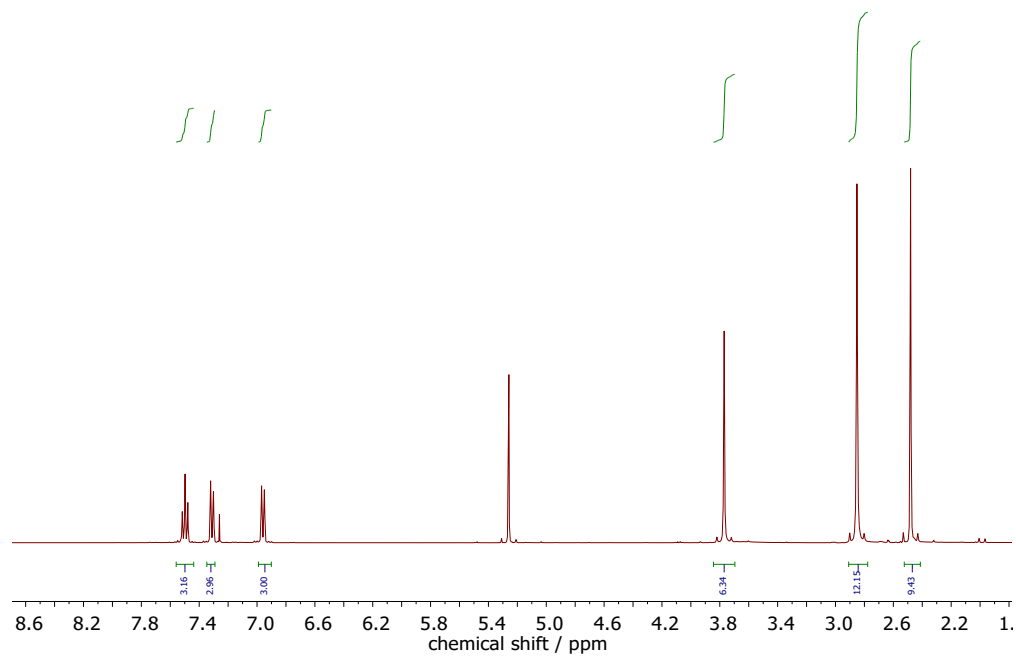


Figure S1 ¹H NMR (400 MHz, CDCl₃, 296 K) of L^{1a}.

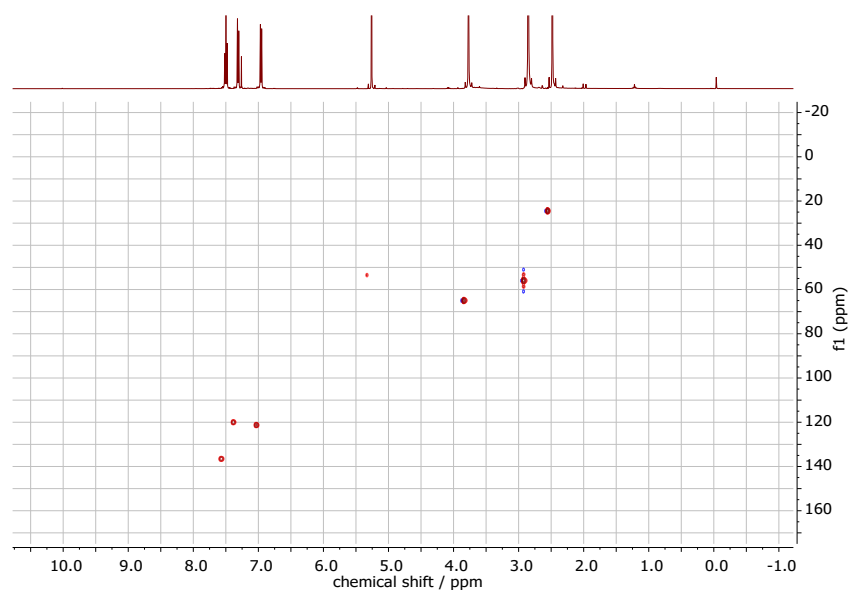


Figure S2 ¹H-¹³C phase-encoded HSQC NMR (400 MHz, CDCl₃, 296 K) of L^{1a}.

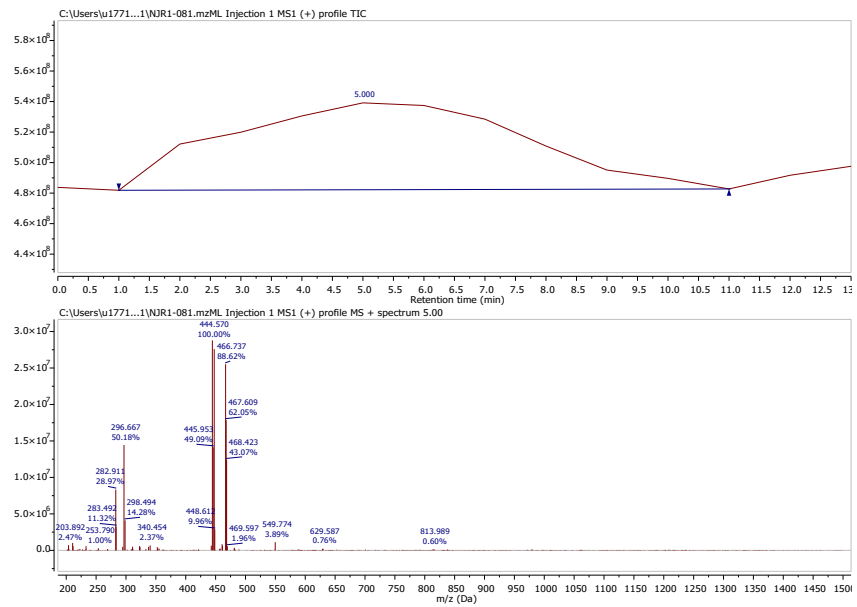
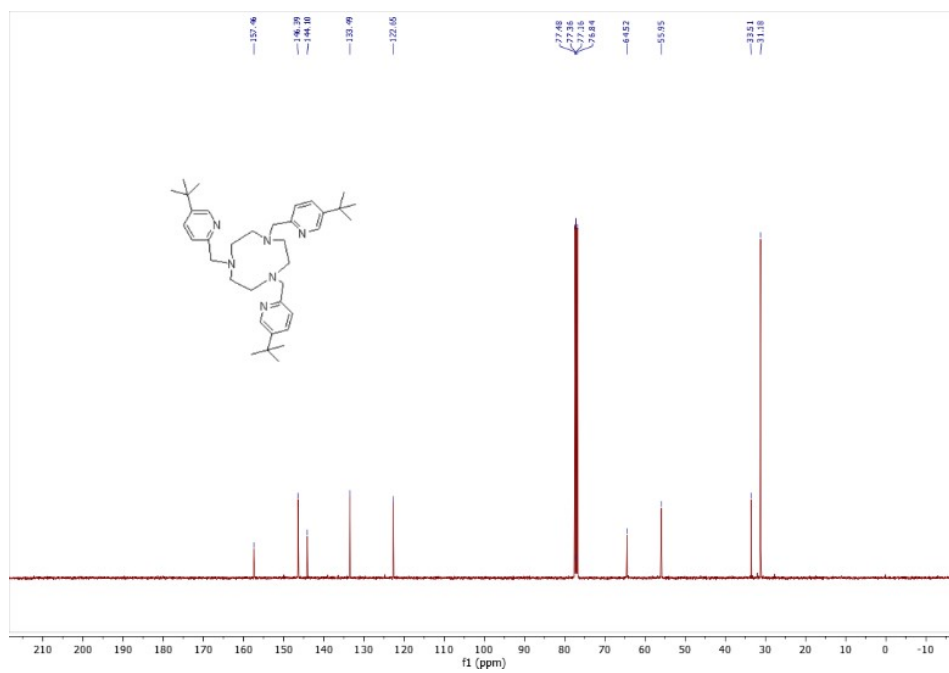
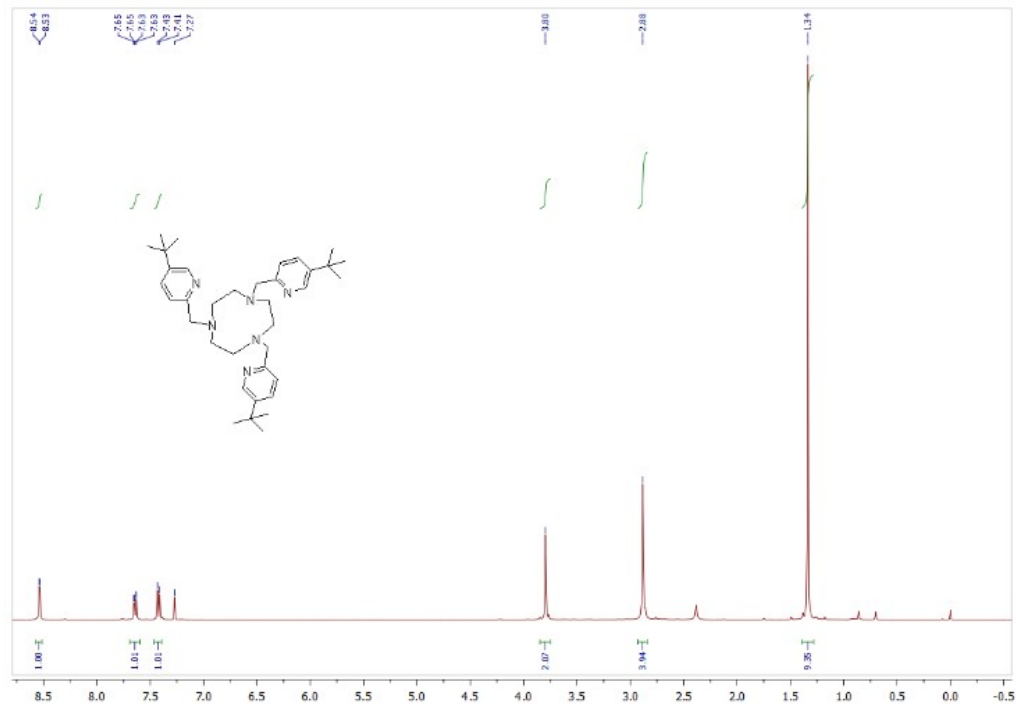


Figure S3 LRMS ES(+) of **L^{1a}**.

Ligand L^{1b}



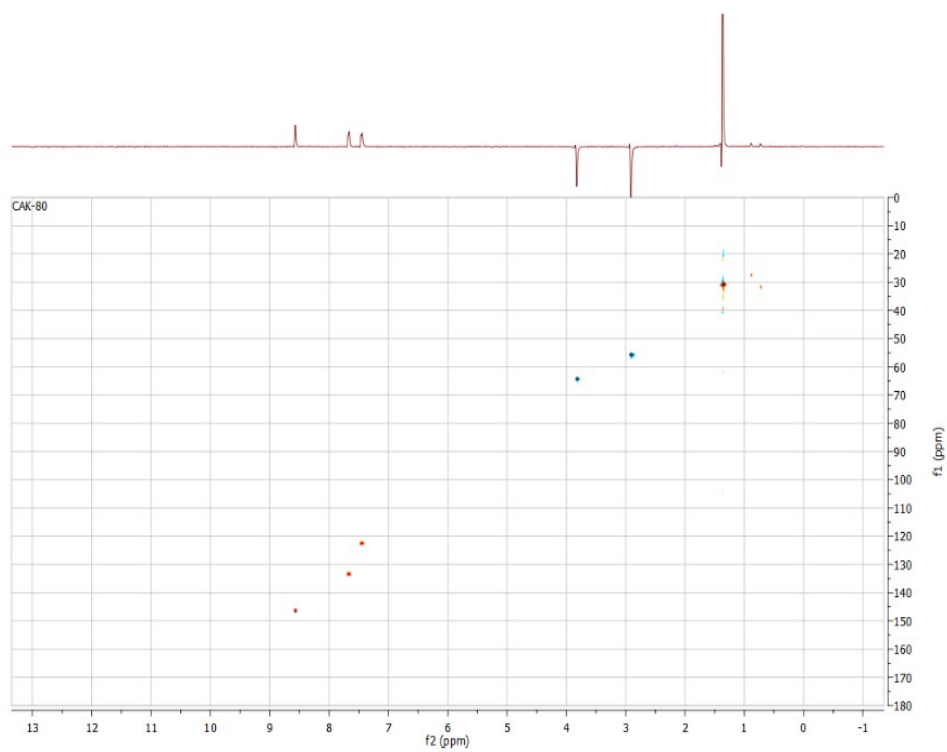


Figure S6 ^1H - ^{13}C phase-encoded HSQC NMR (400 MHz, CDCl_3 , 296 K) of **L^{1b}**.

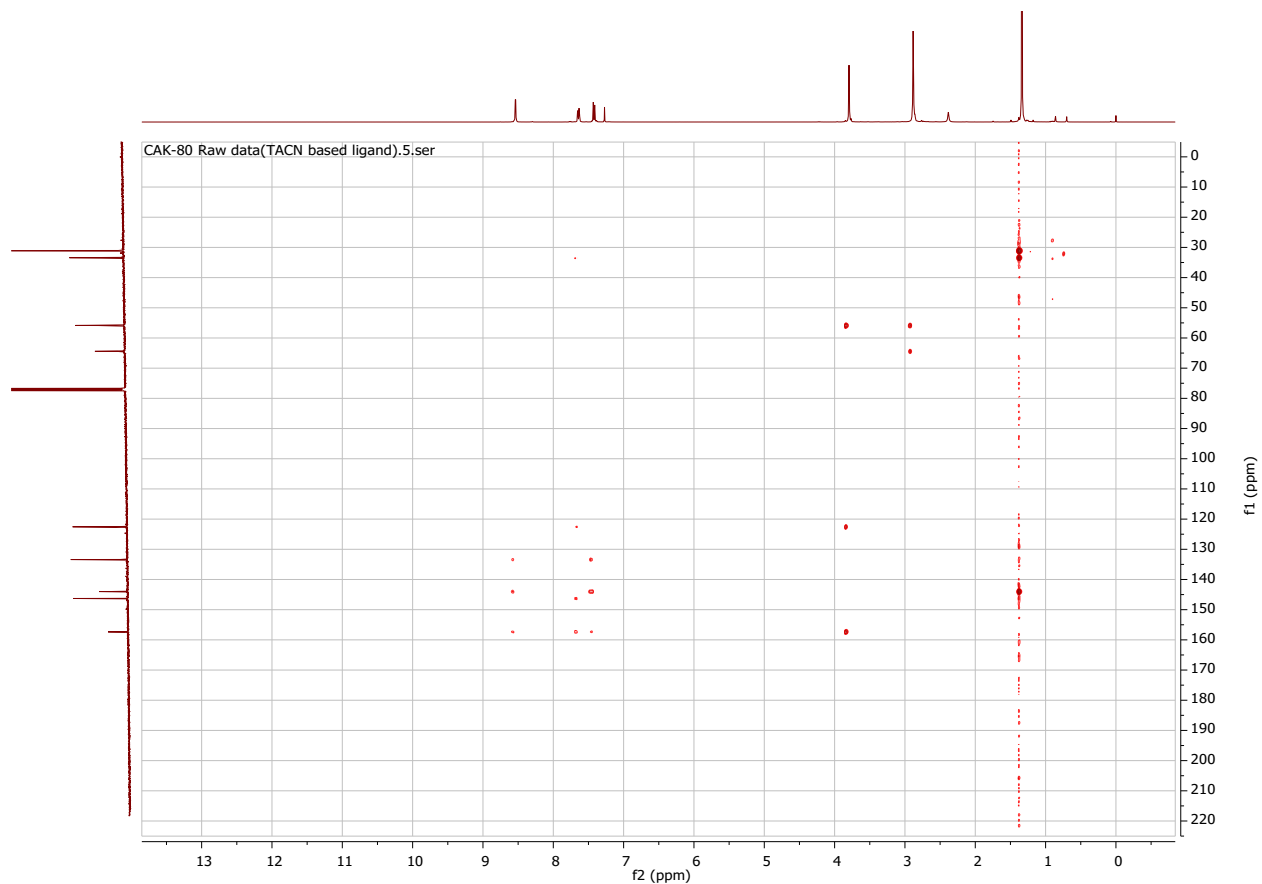


Figure S7 ^1H - ^{13}C HMBC NMR (400 MHz, CDCl_3 , 296 K) of **L^{1b}**.

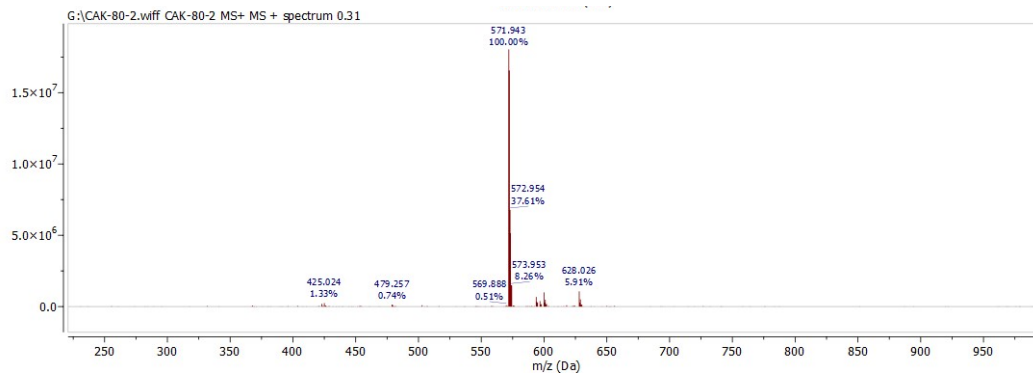


Figure S8 LRMS ES(+) of **L^{1b}**.

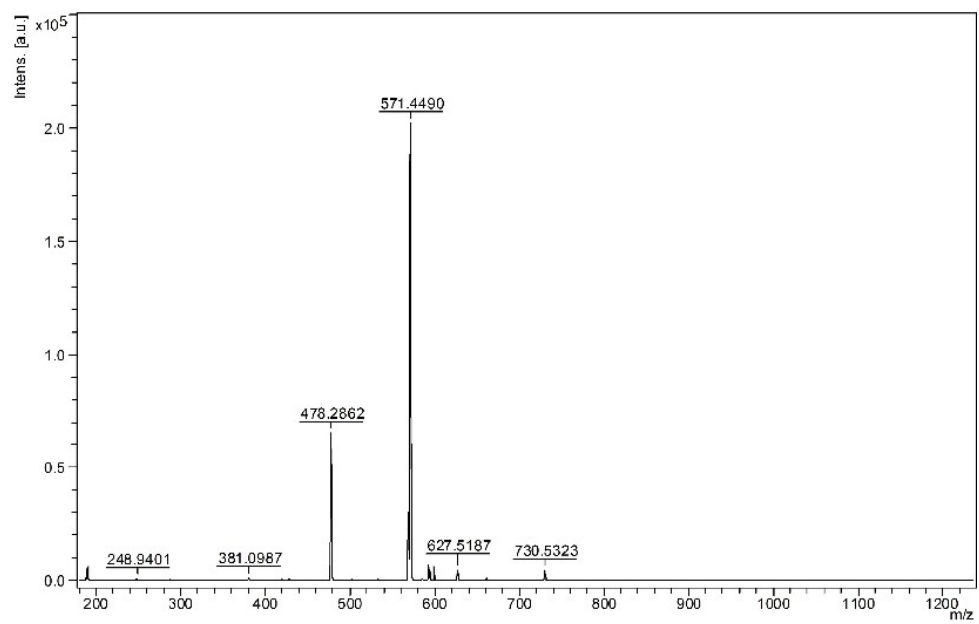


Figure S9 HRHM MALDI-TOF(+) of **L^{1b}**.

Ligand **L^{2a}**

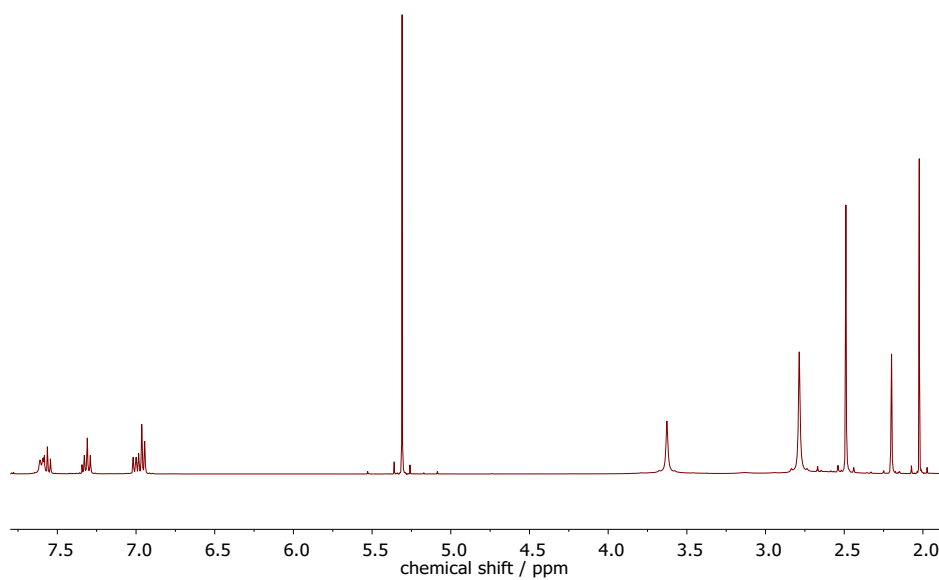


Figure S10 ¹H NMR (400 MHz, CDCl₃, 296 K) of **L^{2a}**

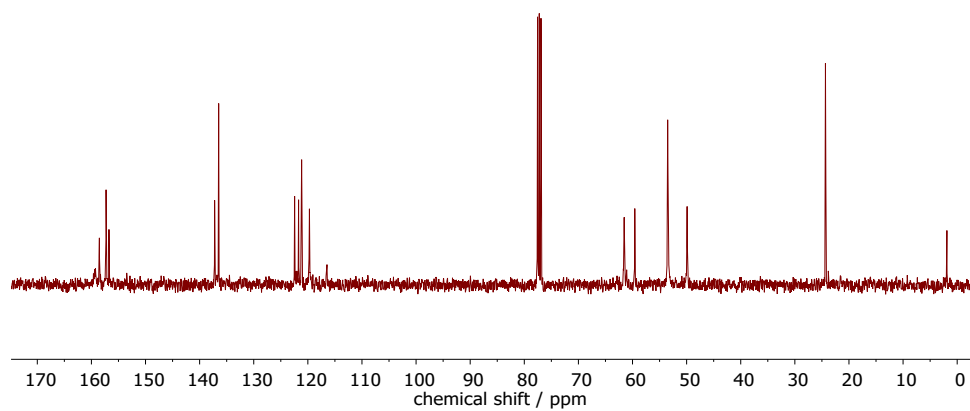


Figure S11 ¹³C {¹H} NMR (400 MHz, CDCl₃, 296 K) of **L^{2a}**

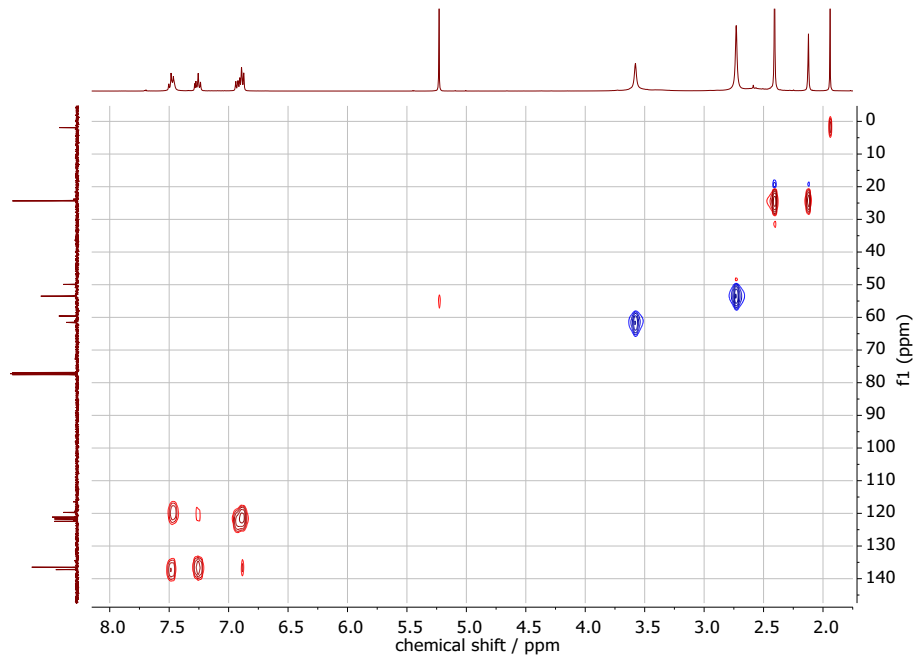


Figure S12 ^1H - ^{13}C phase-encoded HSQC NMR (400 MHz, CDCl_3 , 296 K) of L^{2a} .

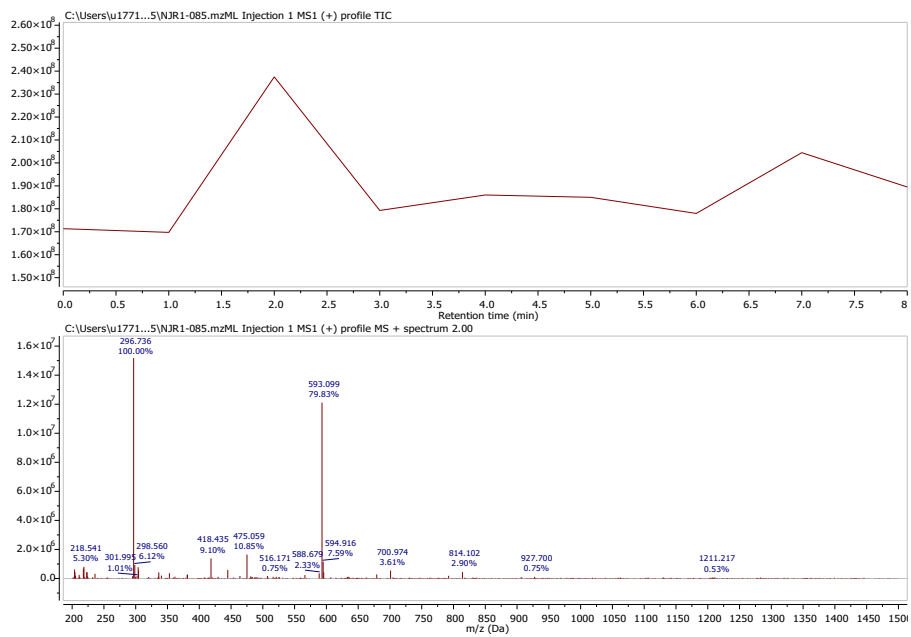


Figure S13 LRMS ES(+) of L^{2a} .

Ligand **L^{2b}**

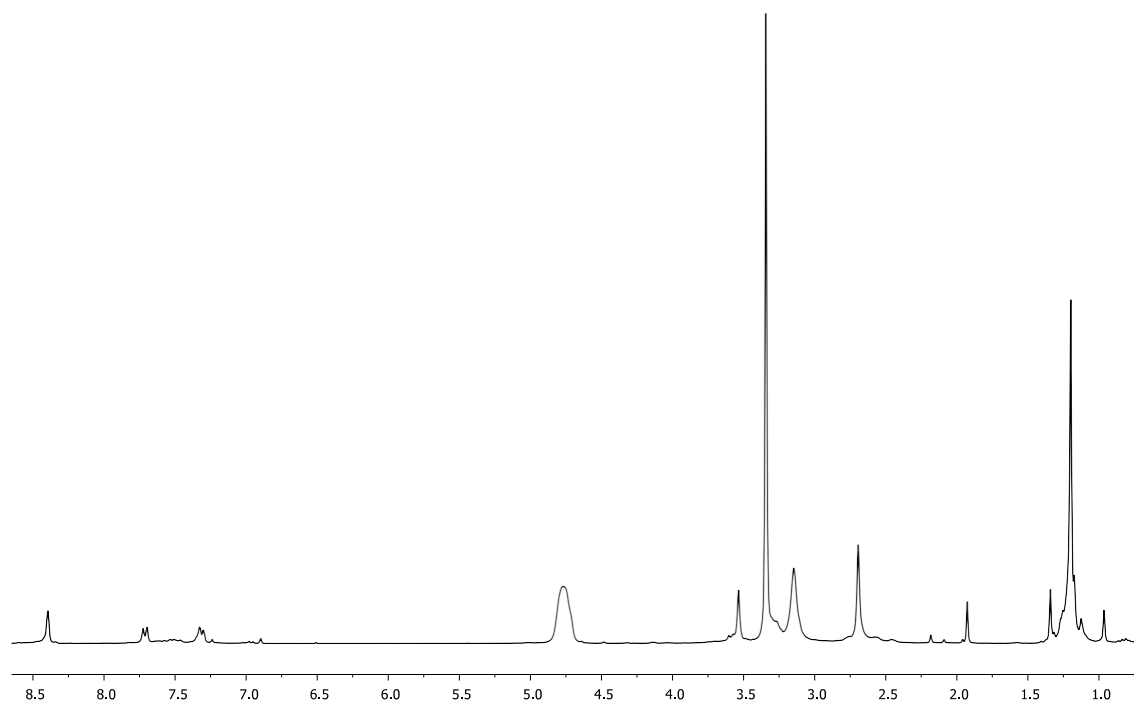


Figure S14 ¹H NMR (300 MHz, CDCl₃, 298 K) of **L^{2b}**

$[\text{MnL}^{1a}]\text{Cl}_2$
NJR1-135.1.fid
NJR1-135 Mn-TACN(6MePy)3Cl2

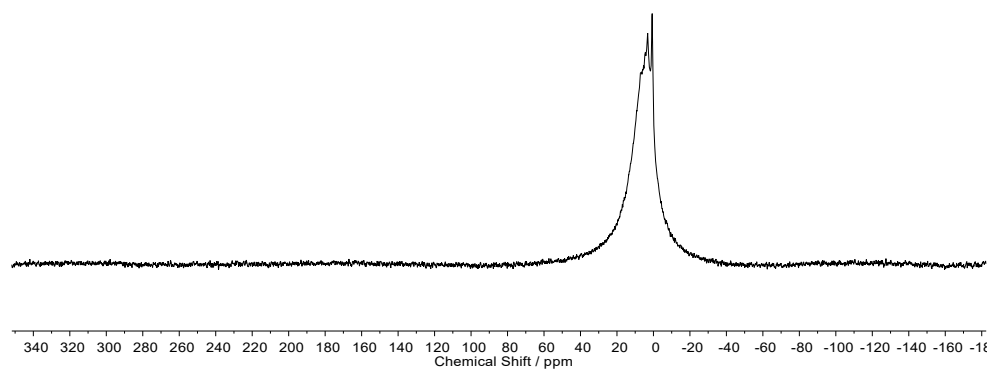


Figure S15 ^1H NMR (80 MHz, D_2O , 300 K) of $[\text{MnL}^{1a}]\text{Cl}_2$

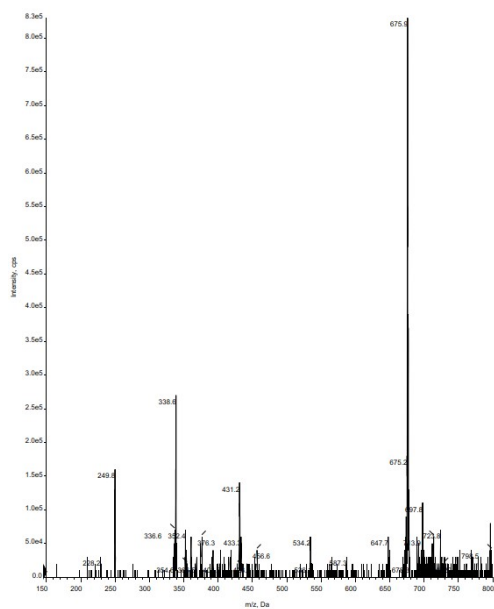


Figure S.16 LRMS ES(+) of $[\text{MnL}^{1a}]\text{Cl}_2$

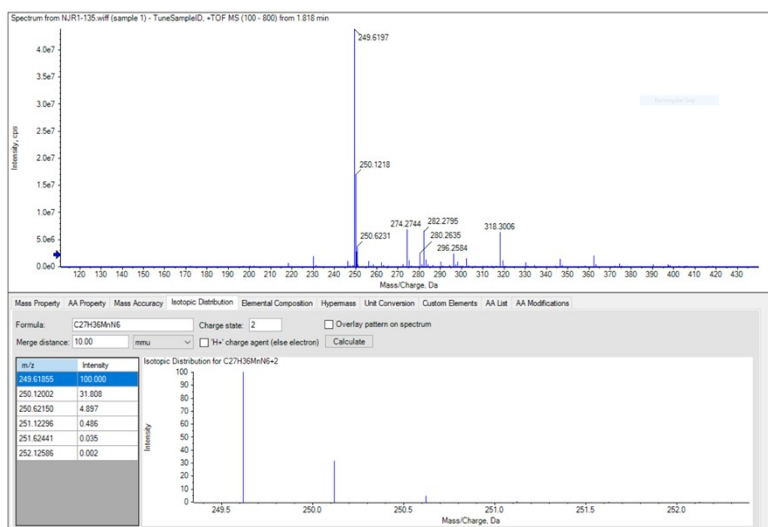


Figure S17 HRMS ES(+) of $[\text{MnL}^{1a}]\text{Cl}_2$

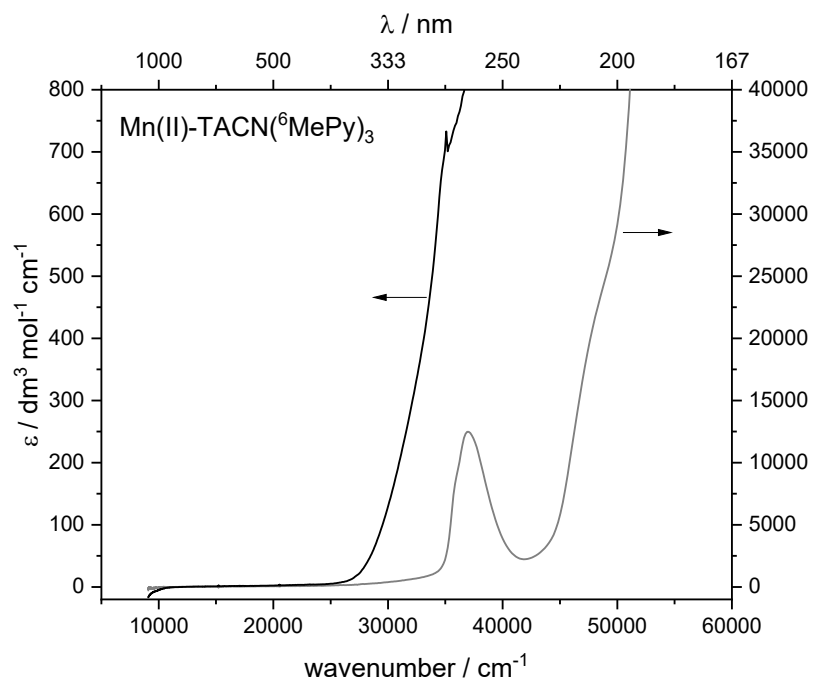


Figure S18 UV-Vis Photoabsorption Spectrum of $[\text{MnL}^{1a}]\text{Cl}_2$ in water (measured at 3 mM and 30 μM).

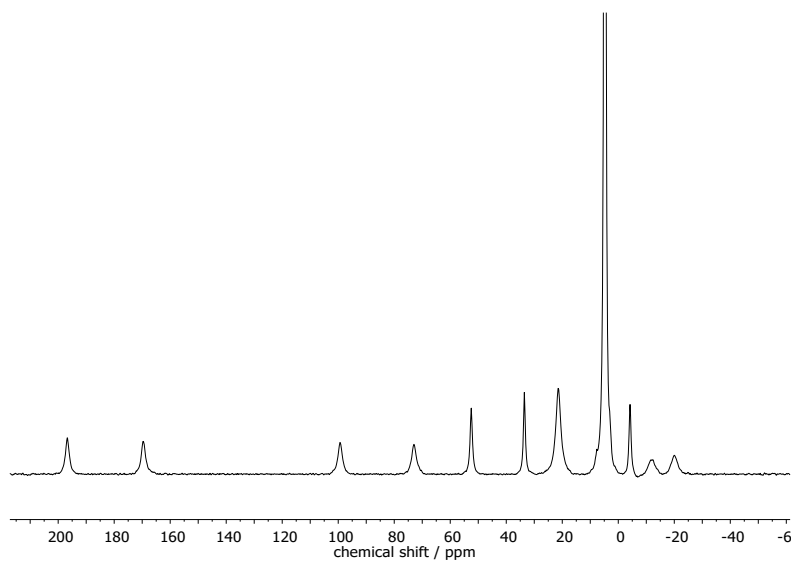


Figure S19 ^1H NMR (80 MHz, D_2O , 300 K) of $[\text{FeL}^{1a}]\text{Cl}_2$

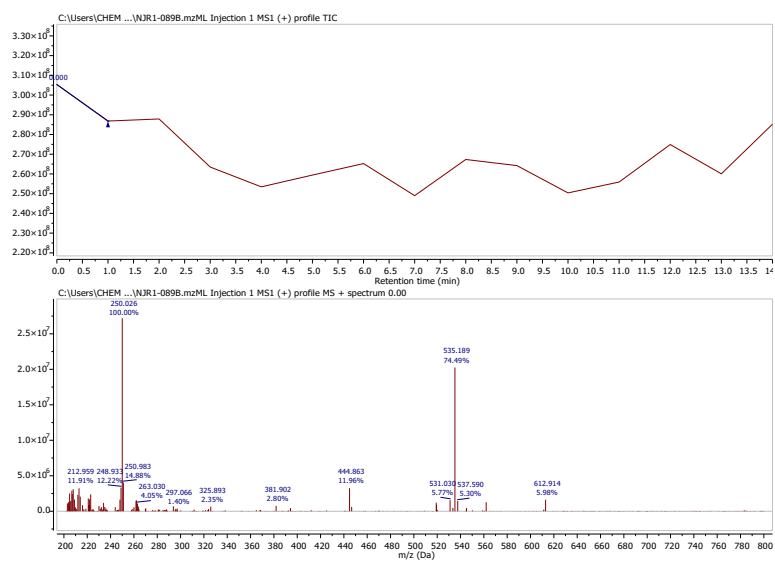


Figure S20 LRMS ES(+) of $[\text{FeL}^{1a}]\text{Cl}_2$

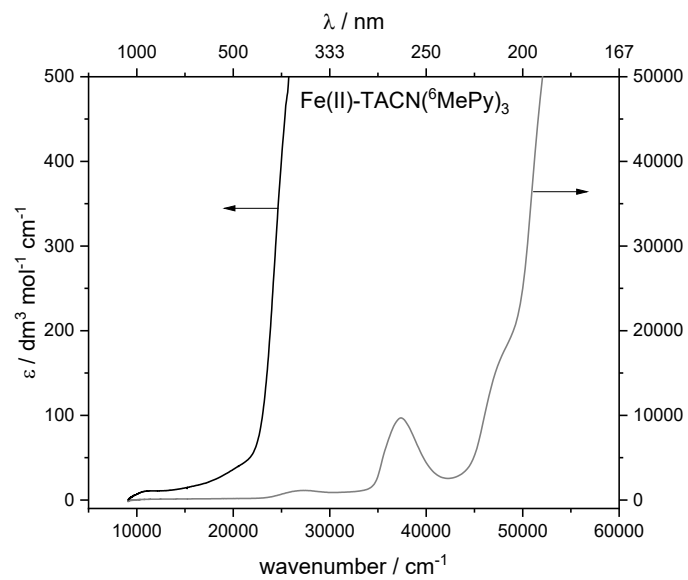


Figure S21 UV-Vis Photoabsorption Spectrum of [FeL^{1a}]Cl₂ in water (measured at 3 mM and 30 μM).

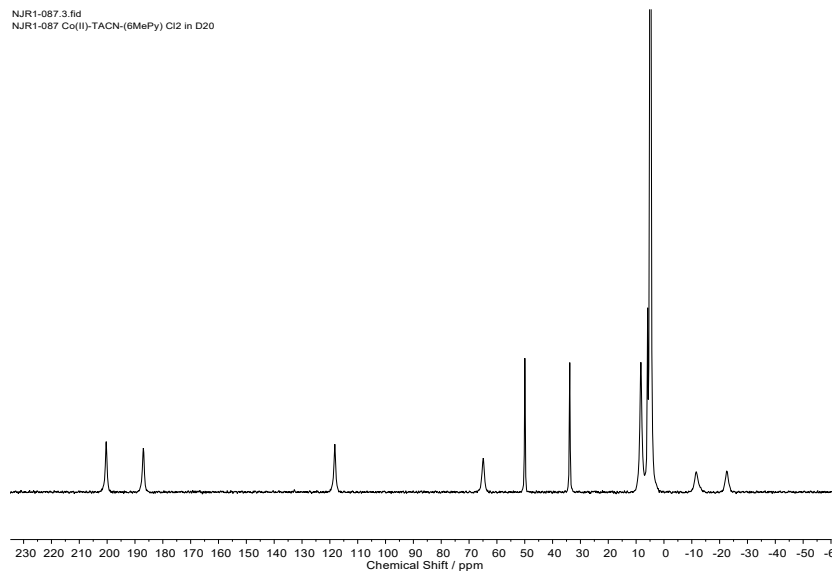


Figure S22 ^1H NMR (80 MHz, D_2O , 300 K) of $[\text{CoL}^{1a}]\text{Cl}_2$

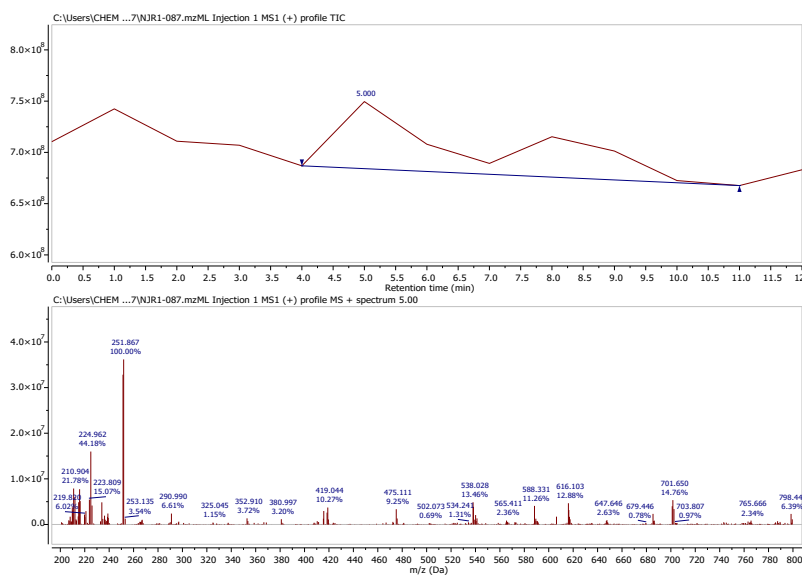


Figure S23 LRMS ES(+) of $[\text{CoL}^{1a}]\text{Cl}_2$

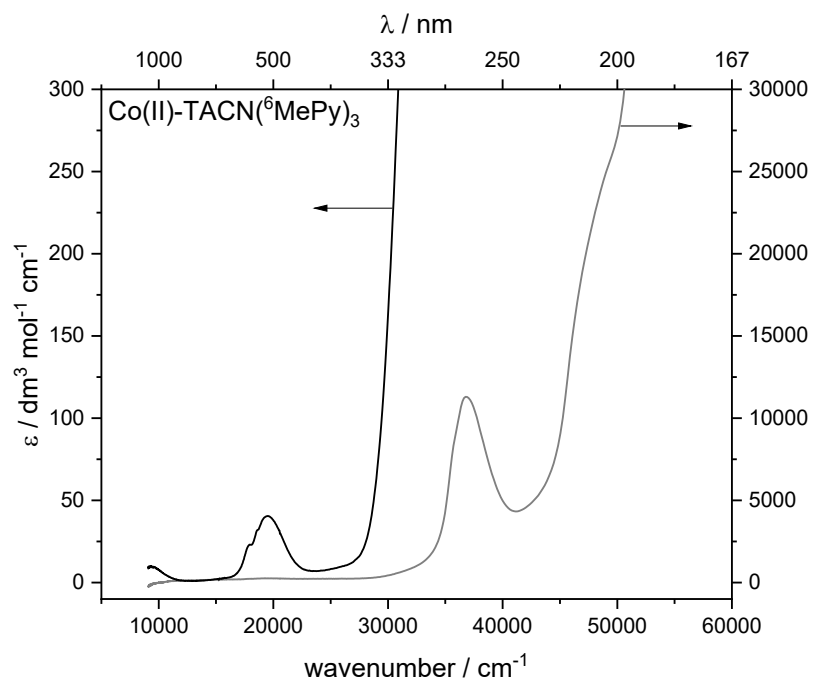


Figure S24 UV-Vis Photoabsorption Spectrum of $[\text{CoL}^{1a}]\text{Cl}_2$ in water (measured at 3 mM and 30 μM).

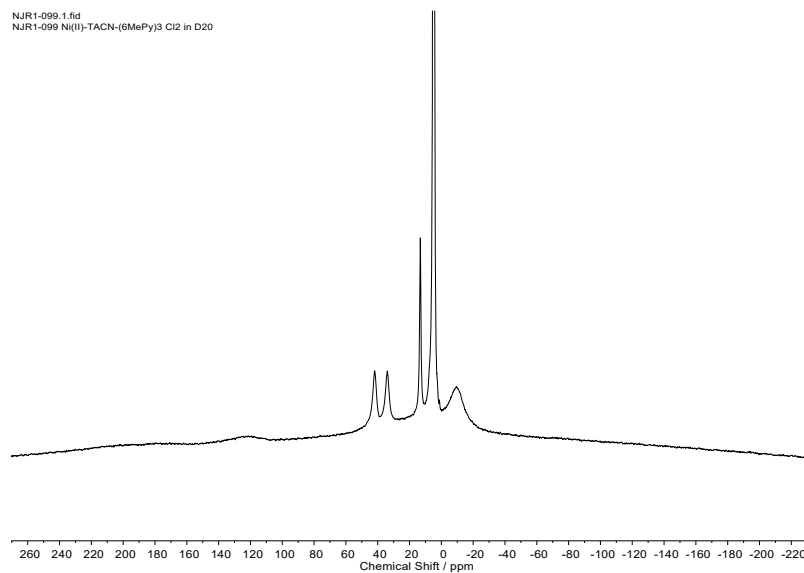


Figure S25 ^1H NMR (80 MHz, D_2O , 300 K) of $[\text{NiL}^{1a}]\text{Cl}_2$

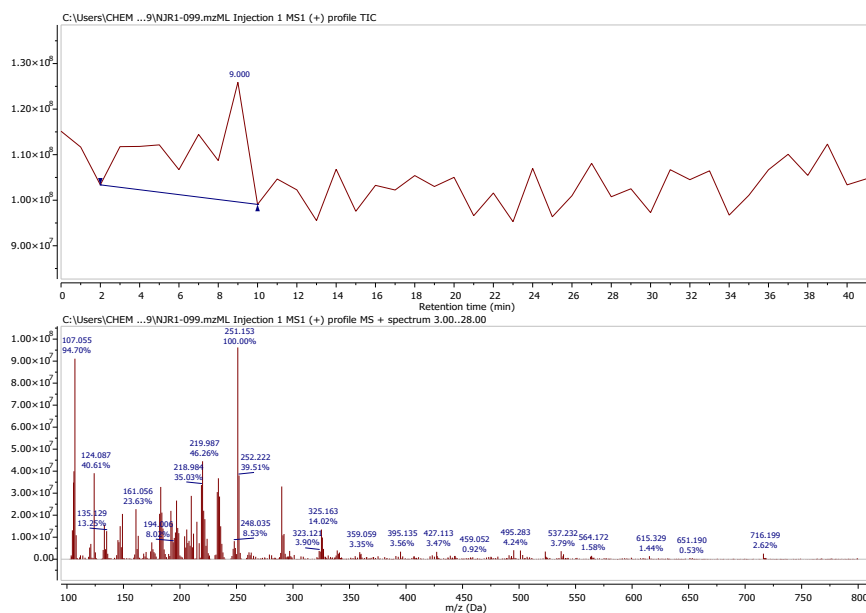


Figure S26 LRMS ES(+) of $[\text{NiL}^{1a}]\text{Cl}_2$

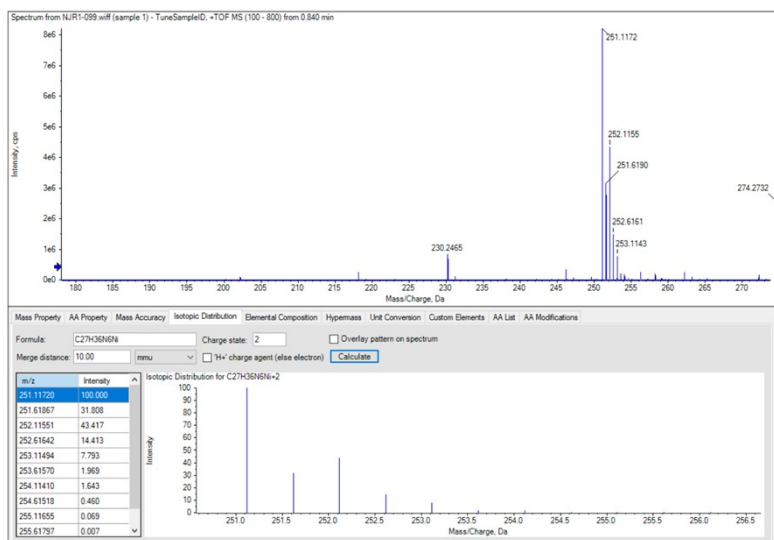


Figure S27 HRMS ES(+) of $[\text{NiL}^{1a}]\text{Cl}_2$

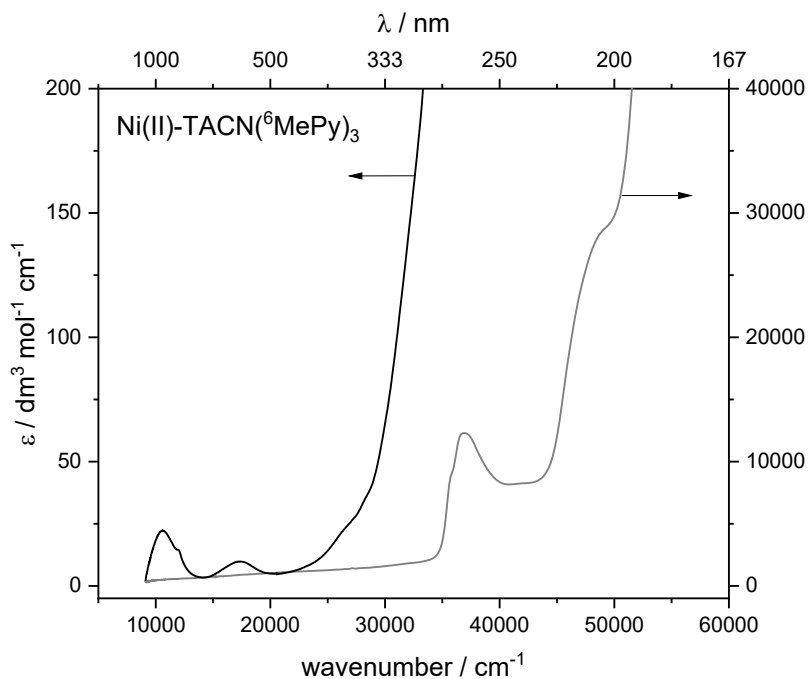


Figure S28 UV-Vis Photoabsorption Spectrum of $[\text{NiL}^{1a}]\text{Cl}_2$ in water (measured at 3 mM and 30 μM).

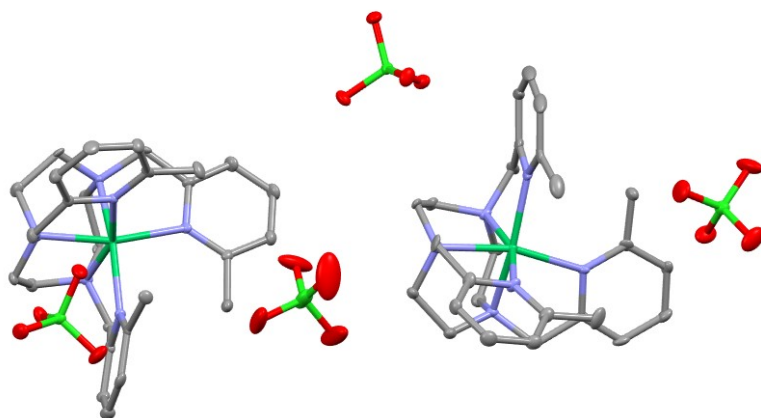


Figure S29 Asymmetric unit of the crystal structure of [NiL^{1a}](ClO₄)₂, displayed as a thermal ellipsoid plot (50% probability) with H atoms removed for clarity. The asymmetric unit contains $\Lambda(\delta\delta\delta)$ and $\Delta(\lambda\lambda\lambda)$ conformational isomers. X-ray crystallography performed at 100 K.

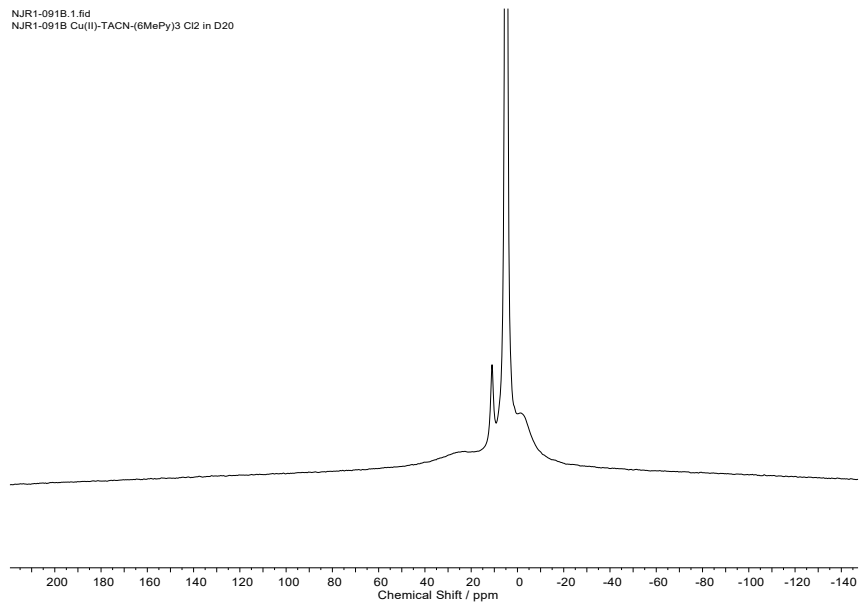


Figure S30 ^1H NMR (80 MHz, D_2O , 300 K) of $[\text{CuL}^{1a}]\text{Cl}_2$

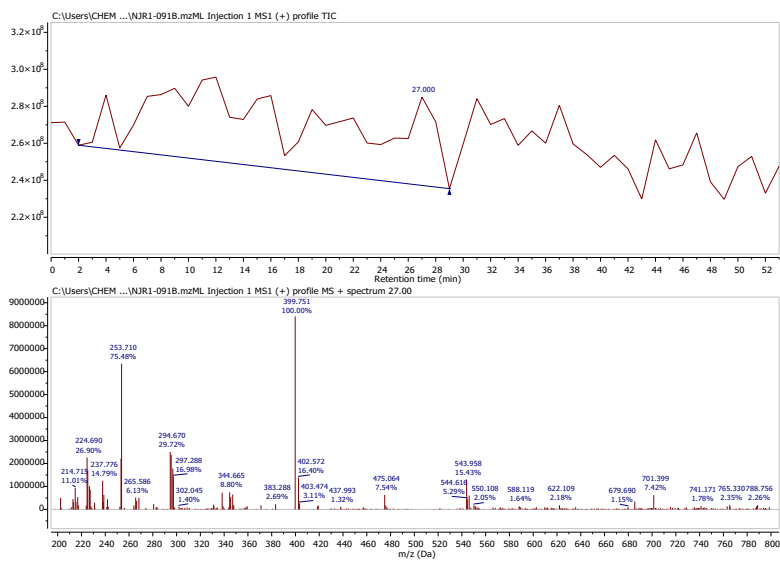


Figure S31 LRMS ES(+) of $[\text{CuL}^{1a}]\text{Cl}_2$

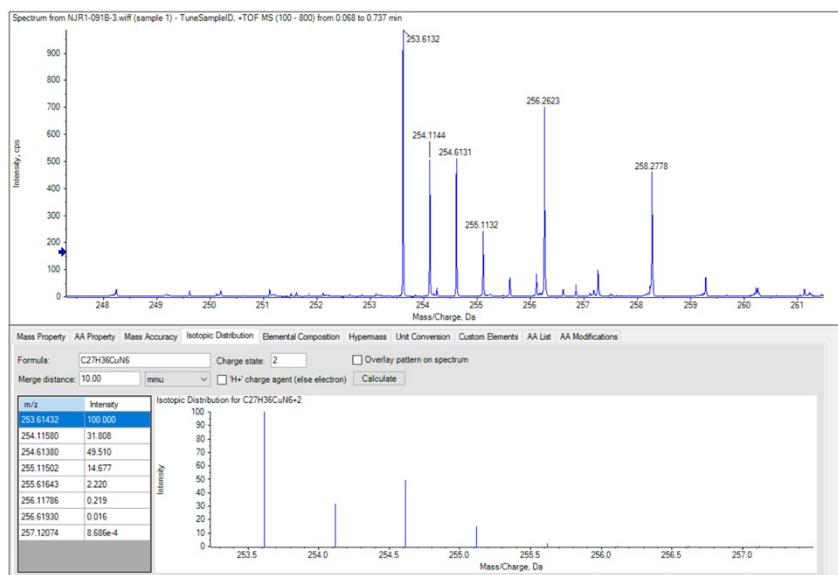


Figure S32 HRMS ES(+) of $[\text{CuL}^{\text{1a}}]\text{Cl}_2$

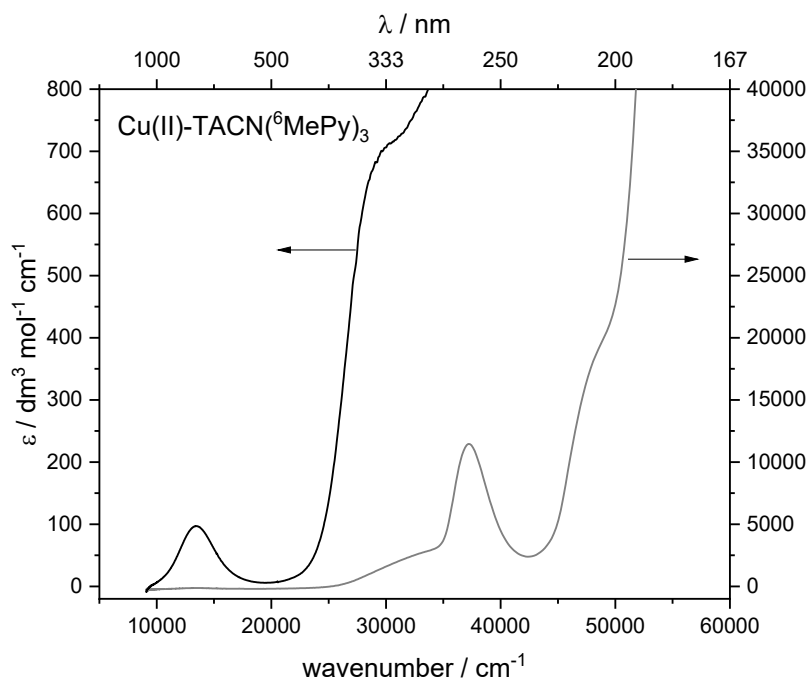


Figure S33 UV-Vis Photoabsorption Spectrum of $[\text{CuL}^{\text{1a}}]\text{Cl}_2$ in water (measured at 3 mM and 30 μM).

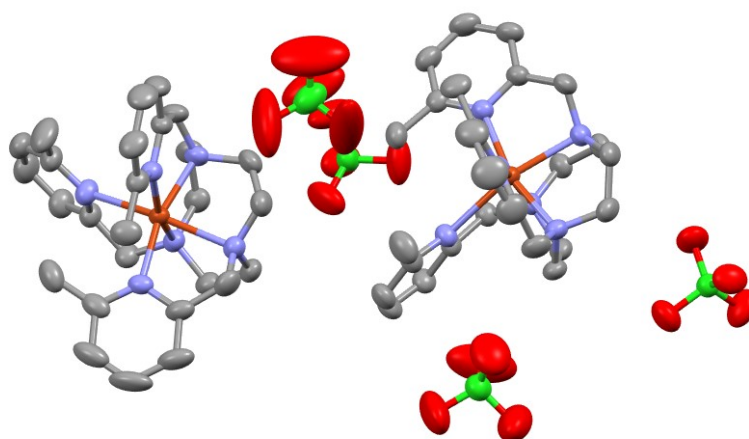


Figure S34. Asymmetric unit of the crystal structure of [CuL^{1a}](ClO₄), displayed as a thermal ellipsoid plot (50% probability) with H atoms removed for clarity. The asymmetric unit contains Δ(λλλ) and Λ(δδδ) conformational isomers. X-ray crystallography performed at 300 K.

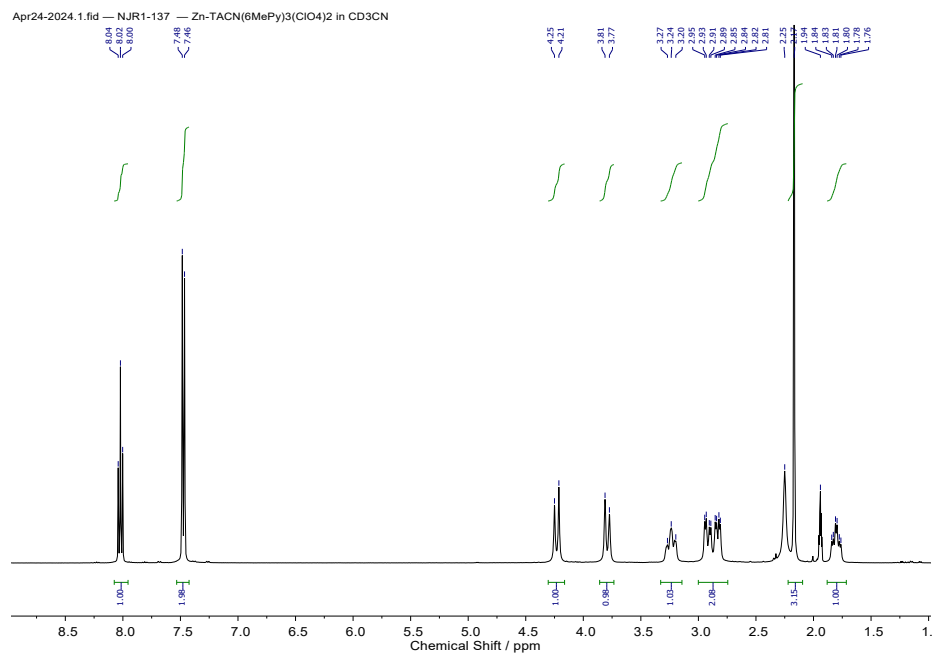
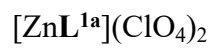


Figure S35 ^1H NMR (400 MHz, CD_3CN , 296 K) of $[\text{ZnL}^{1a}](\text{ClO}_4)_2$

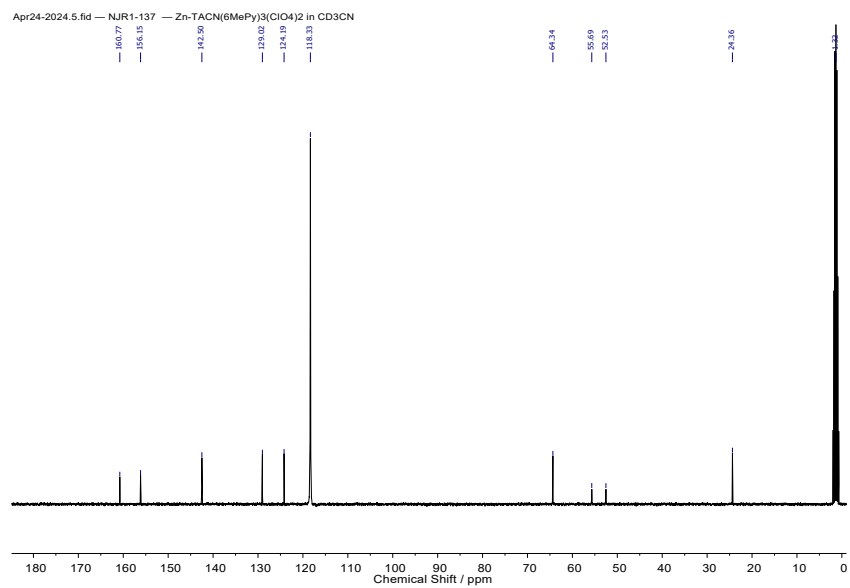


Figure S36 $^{13}\text{C}\{^1\text{H}\}$ NMR (101 MHz, CD_3CN , 296 K) of $[\text{ZnL}^{1a}](\text{ClO}_4)_2$

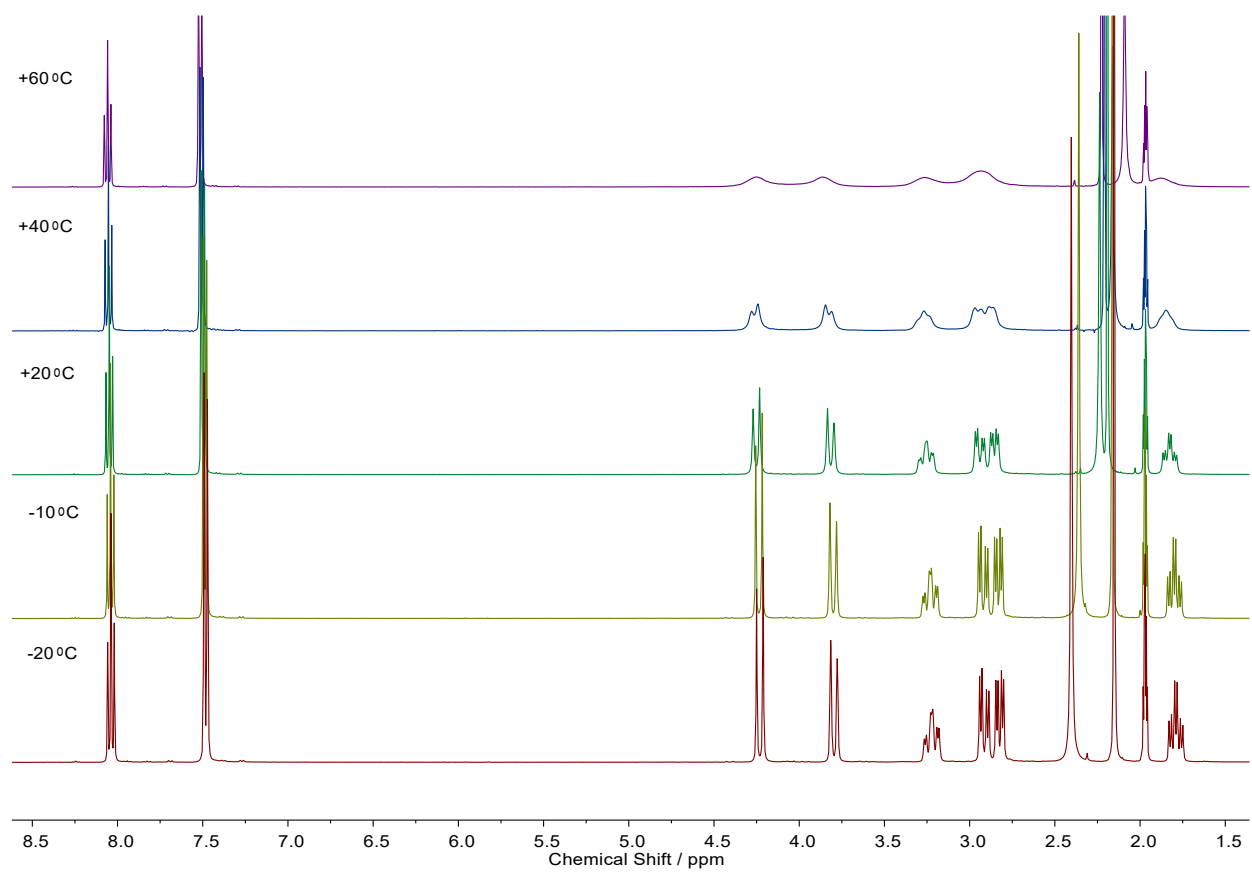


Figure S37 Variable temperature ^1H NMR (400 MHz, CD_3CN) of $[\text{ZnL}^{\text{1a}}](\text{ClO}_4)_2$

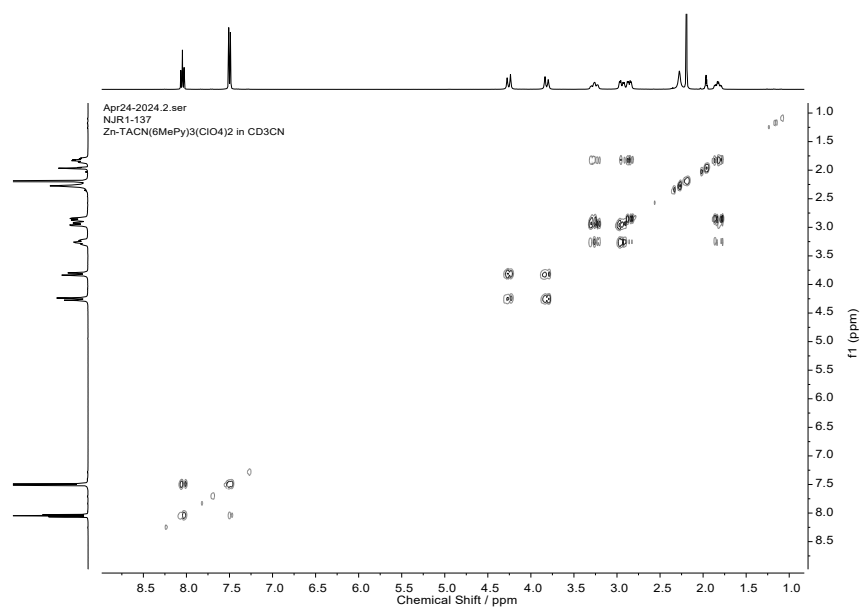


Figure S38 ^1H - ^1H COSY NMR (400 MHz, CD_3CN , 296 K) of $[\text{ZnL}^{1a}](\text{ClO}_4)_2$

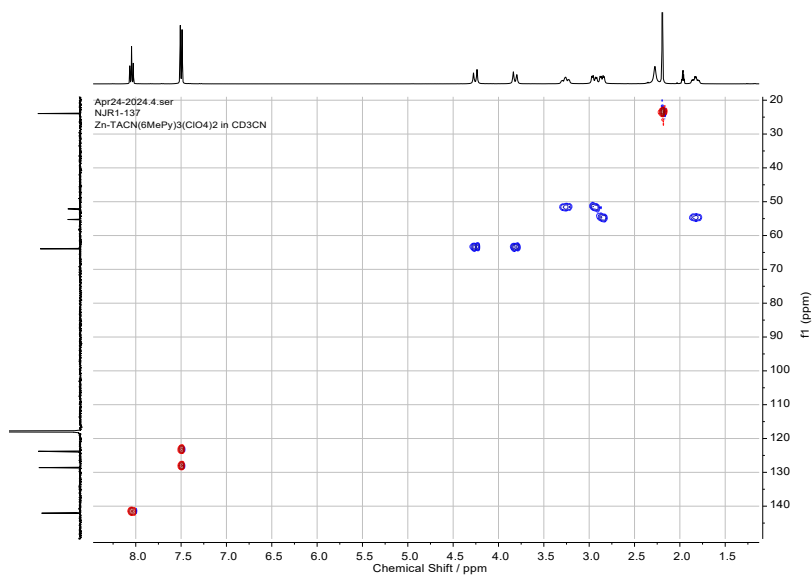


Figure S39 ^1H - ^{13}C HSQC phase-encoded NMR (400 MHz, CD_3CN , 296 K) of $[\text{ZnL}^{1a}](\text{ClO}_4)_2$

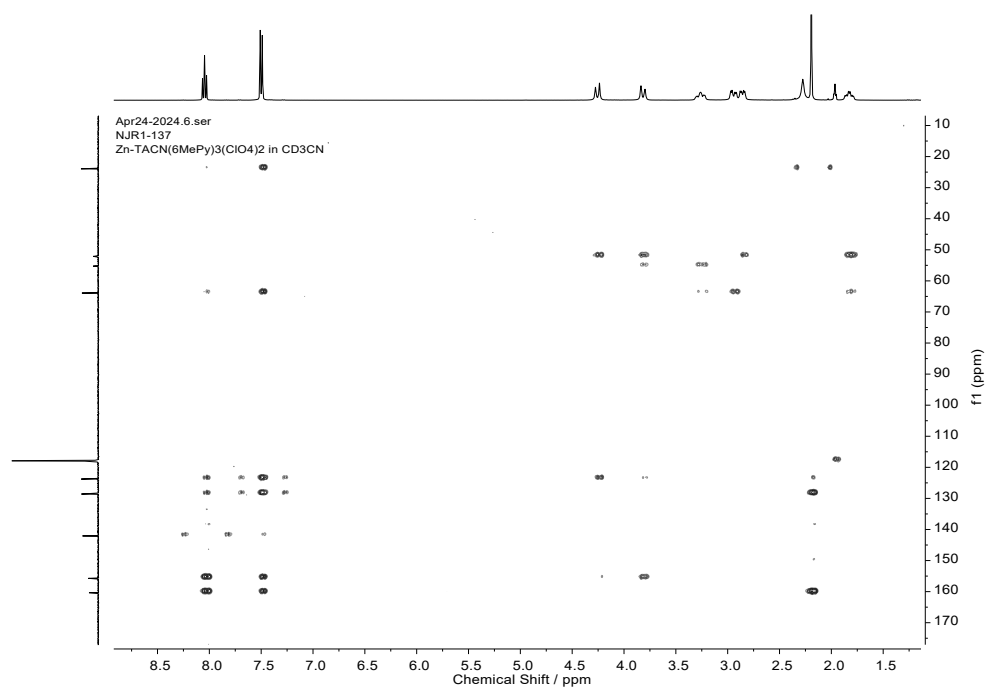


Figure S40 ^1H - ^{13}C HMBC NMR (400 MHz, CD_3CN , 296 K) of $[\text{ZnL}^{1a}](\text{ClO}_4)_2$

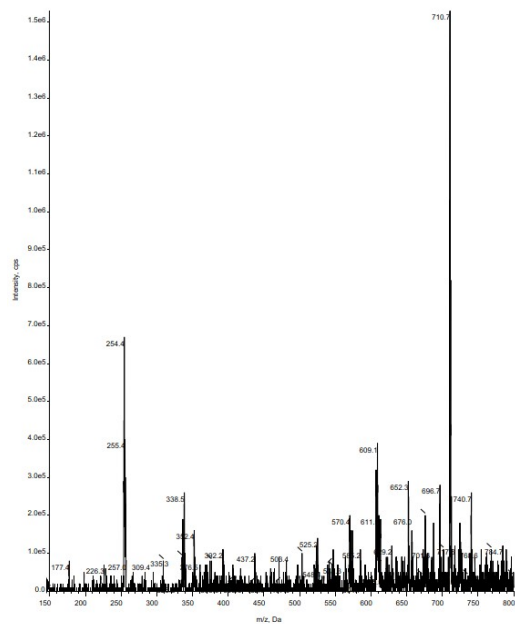


Figure S41 LRMS ES(+) of $[\text{ZnL}^{\text{1a}}](\text{ClO}_4)_2$

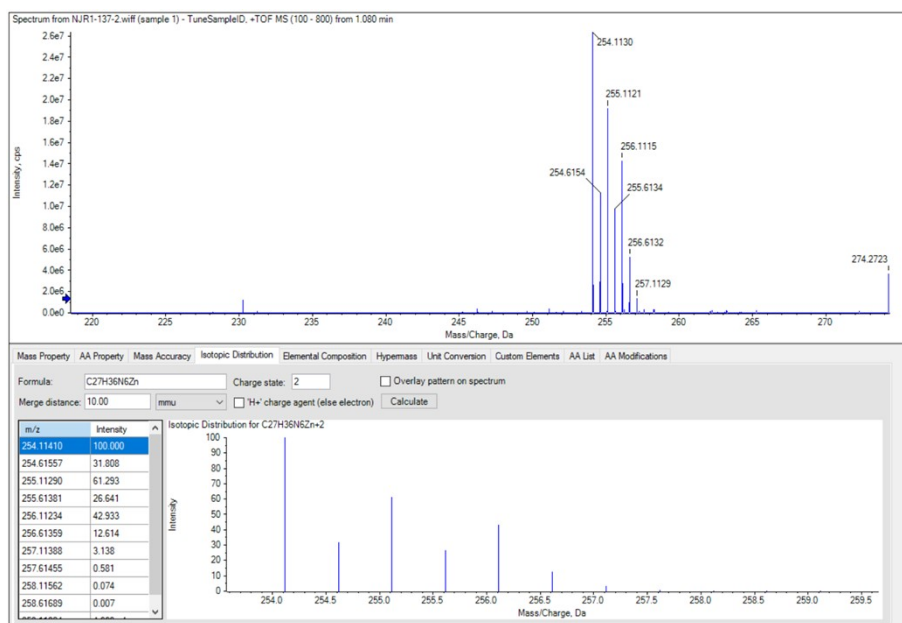


Figure S42 HRMS ES(+) of $[\text{ZnL}^{\text{1a}}](\text{ClO}_4)_2$

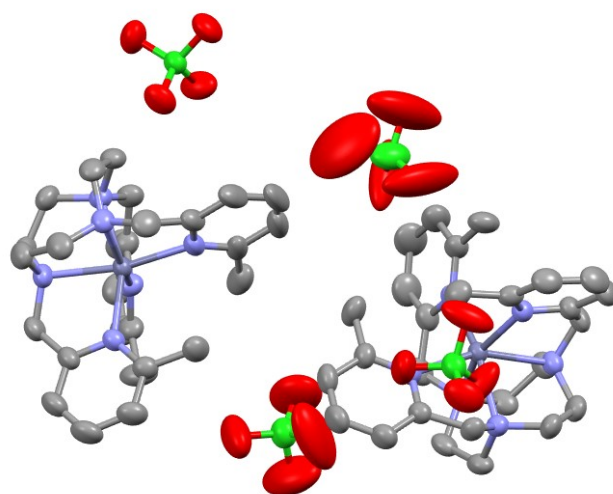


Figure S43. Asymmetric unit of the crystal structure of $[\text{ZnL}^{1\text{a}}](\text{ClO}_4)_2$, displayed as a thermal ellipsoid plot (50% probability), with H atoms removed for clarity. The asymmetric unit contains $\Lambda(\delta\delta\delta)$ conformational isomers. X-ray crystallography performed at 302 K.

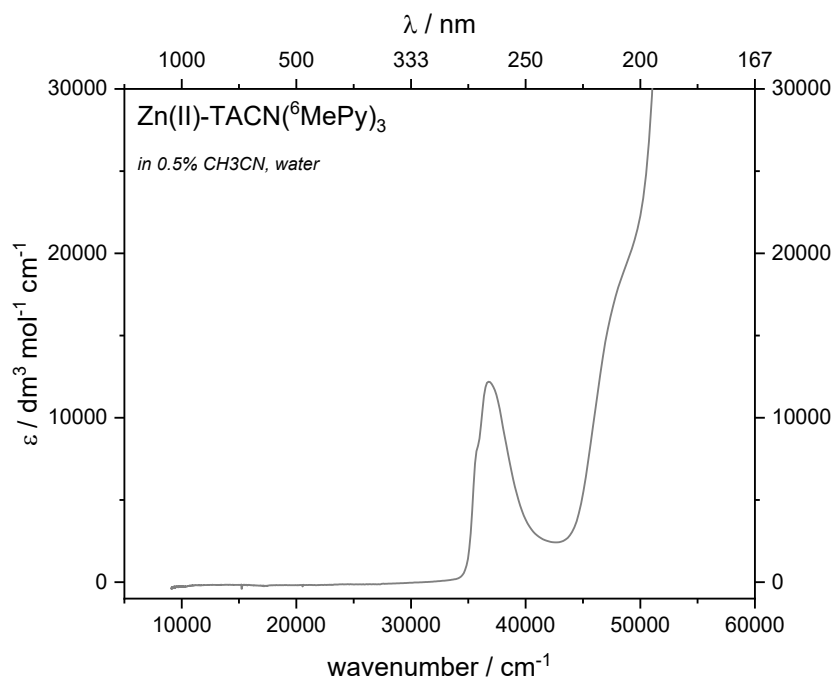


Figure S44 UV-Vis Photoabsorption Spectrum of $[\text{ZnL}^{1\text{a}}](\text{ClO}_4)_2$ in 0.5% CH₃CN, water (measured at 30 μM).

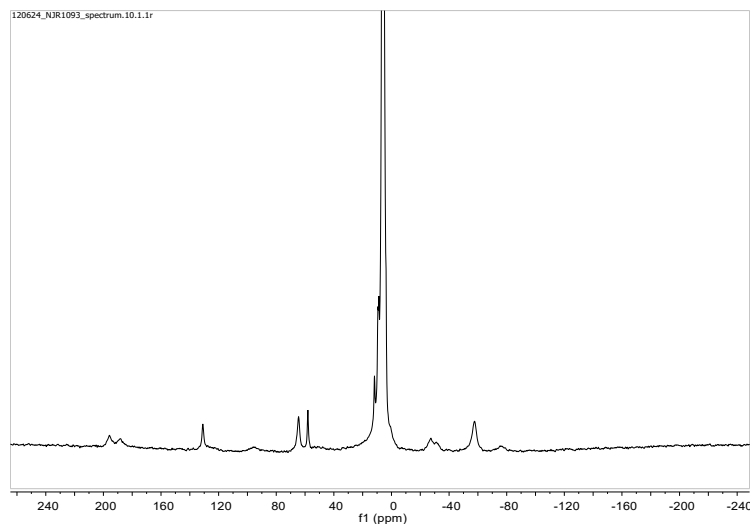


Figure S45 ^1H NMR (80 MHz, D_2O , 300 K) of $[\text{FeL}^{2a}]\text{Cl}_2$

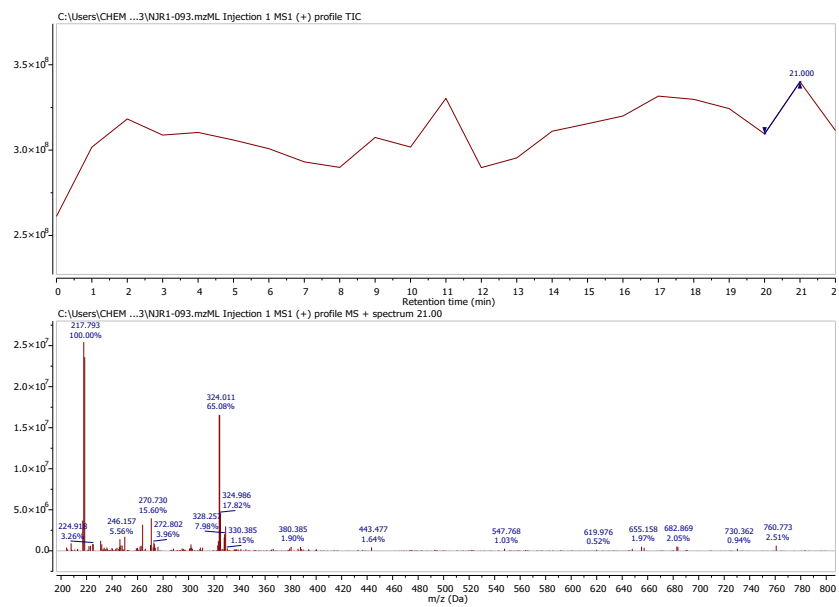


Figure S46 LRMS ES(+) of $[\text{FeL}^{2a}]\text{Cl}_2$

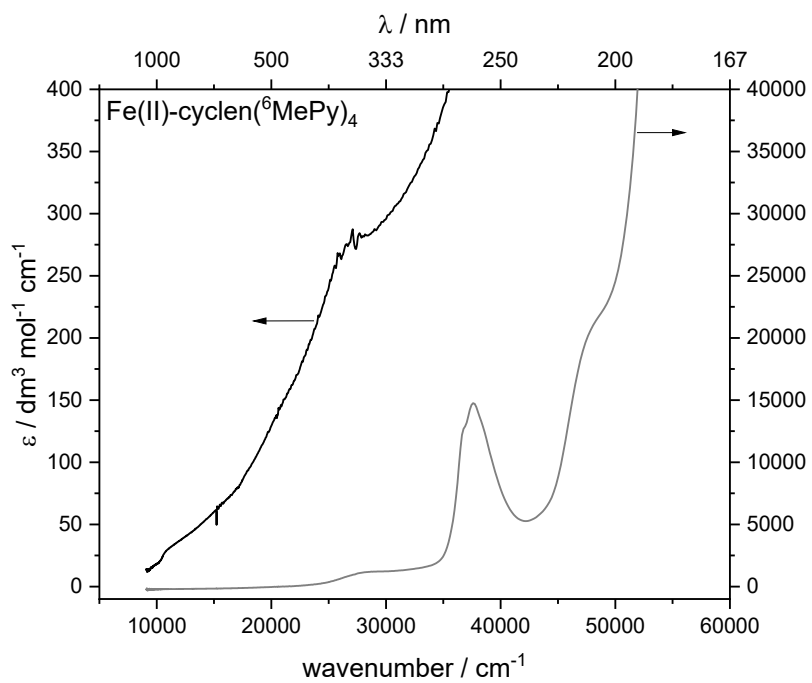


Figure S47 UV-Vis Photoabsorption Spectrum of [FeL^{2a}]Cl₂ in water (measured at 3 mM and 30 μM).

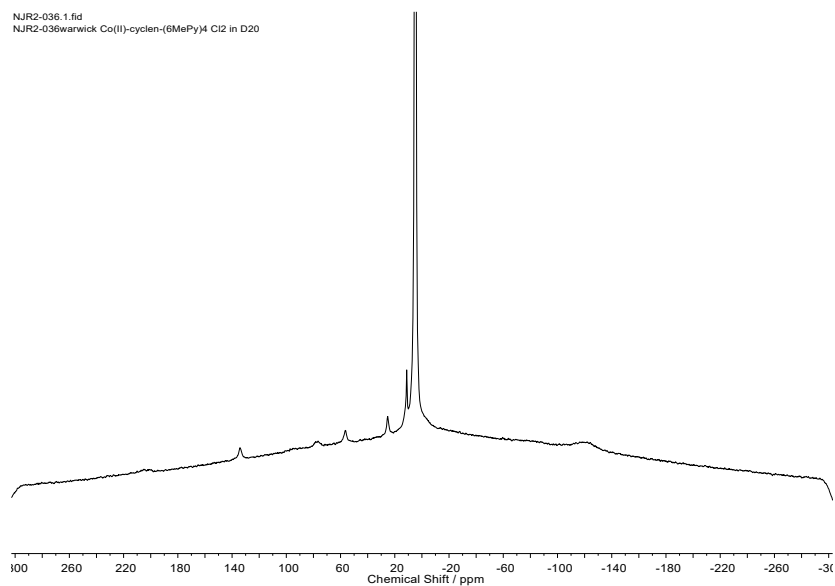


Figure S48 ^1H NMR (80 MHz, D_2O , 300 K) of $[\text{CoL}^{2a}]\text{Cl}_2$

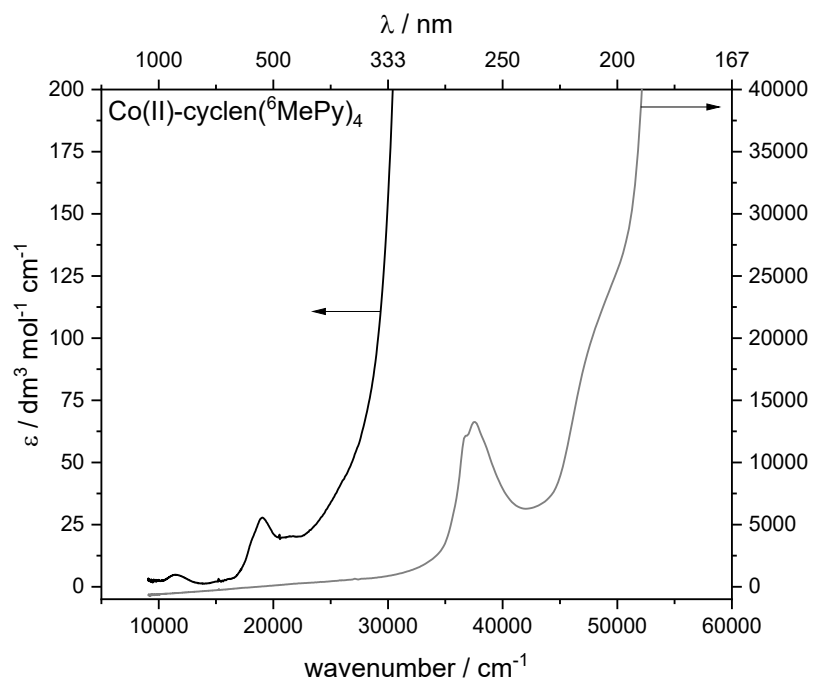


Figure S49 UV-Vis Photoabsorption Spectrum of $[\text{CoL}^{2a}]\text{Cl}_2$ in water (measured at 3 mM and 30 μM).

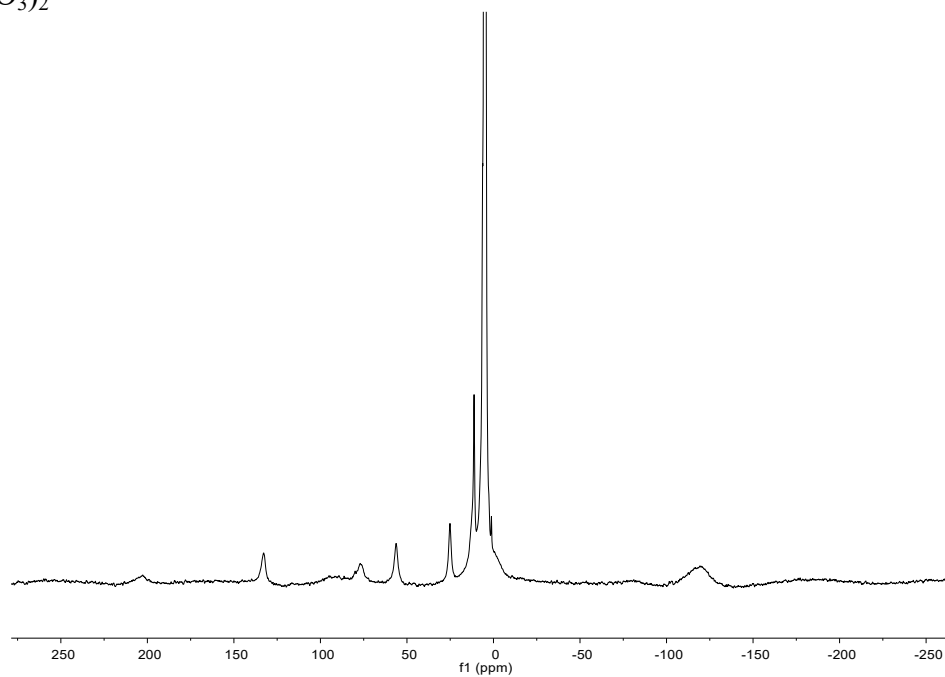
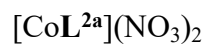


Figure S50 ^1H NMR (80 MHz, D_2O , 300 K) of $[\text{CoL}^{2a}](\text{NO}_3)_2$

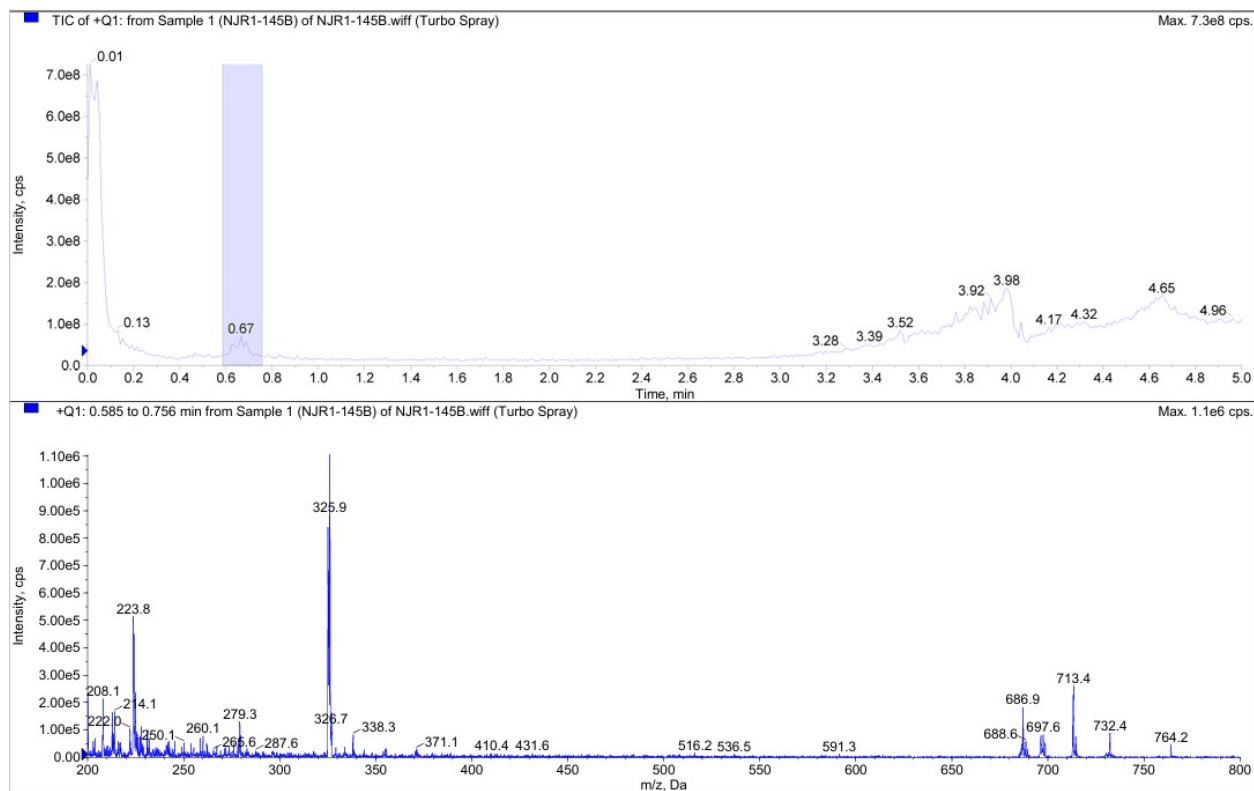


Figure S51 LRMS ES(+) of $[\text{CoL}^{2a}](\text{NO}_3)_2$

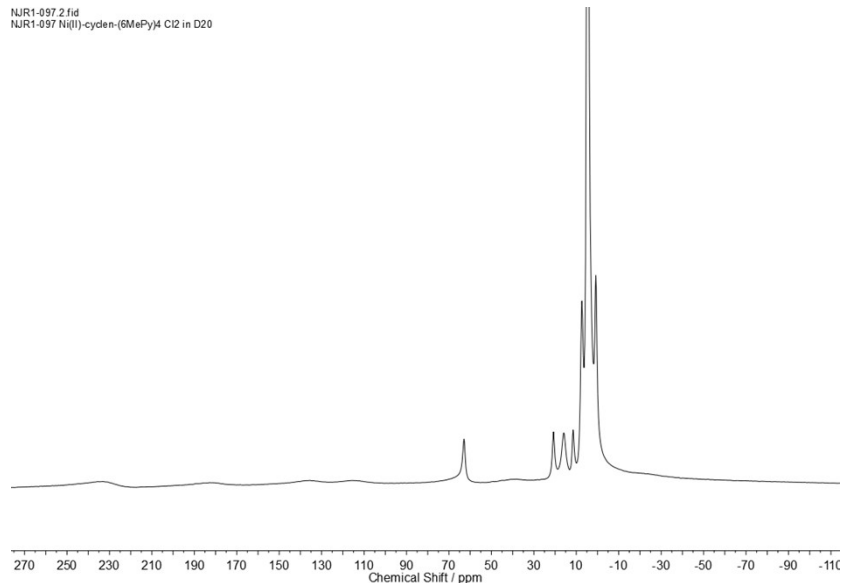


Figure S52 ^1H NMR (80 MHz, D_2O , 300 K) of $[\text{NiL}^{2a}]\text{Cl}_2$

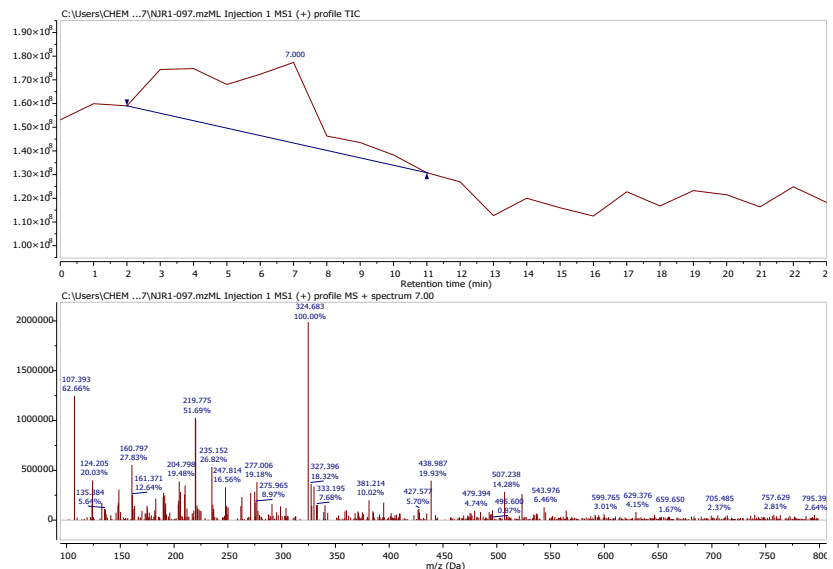


Figure S53 LRMS ES(+) of $[\text{NiL}^{2a}]\text{Cl}_2$

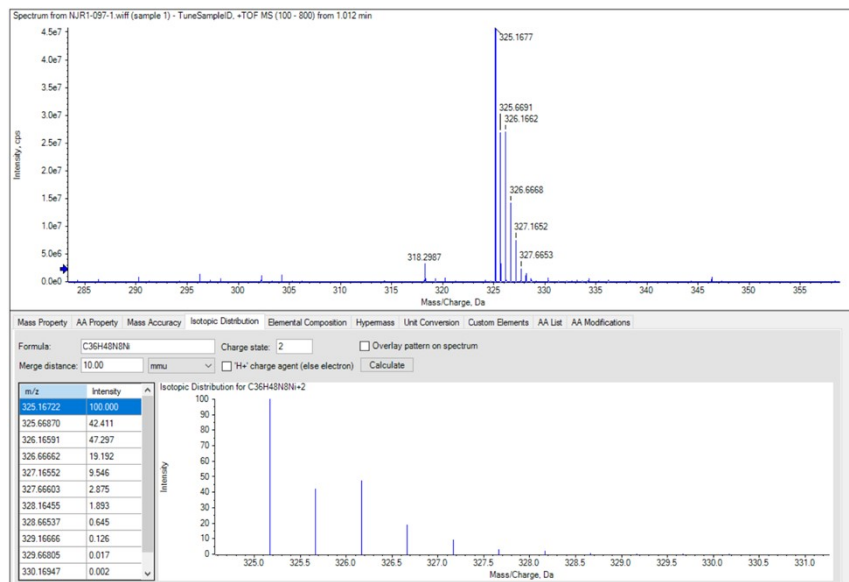


Figure S54 HRMS ES(+) of [NiL^{2a}]Cl₂

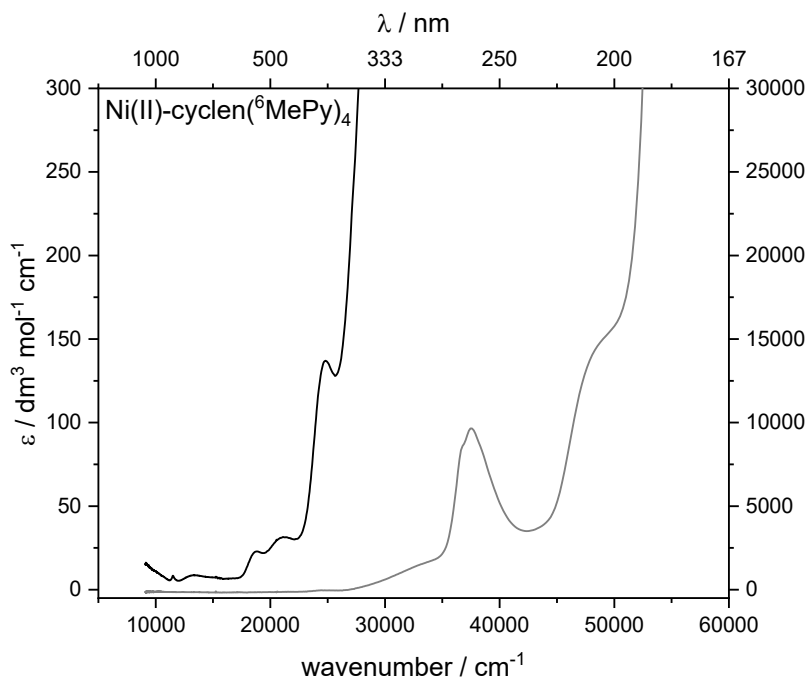


Figure S55 UV-Vis Photoabsorption Spectrum of [NiL^{2a}]Cl₂ in water (measured at 3 mM and 30 μM).

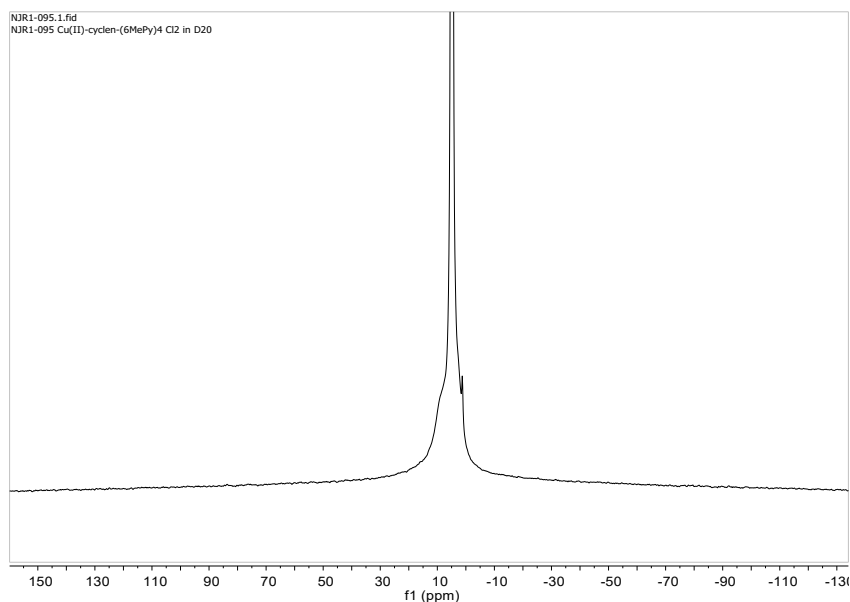


Figure S56 ^1H NMR (80 MHz, D_2O , 300 K) of $[\text{CuL}^{2a}]\text{Cl}_2$

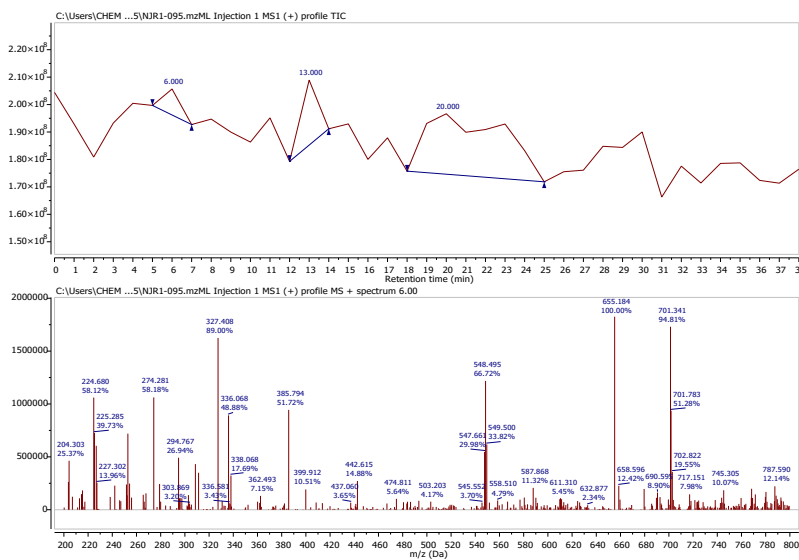


Figure S57 LRMS ES(+) of $[\text{CuL}^{2a}]\text{Cl}_2$

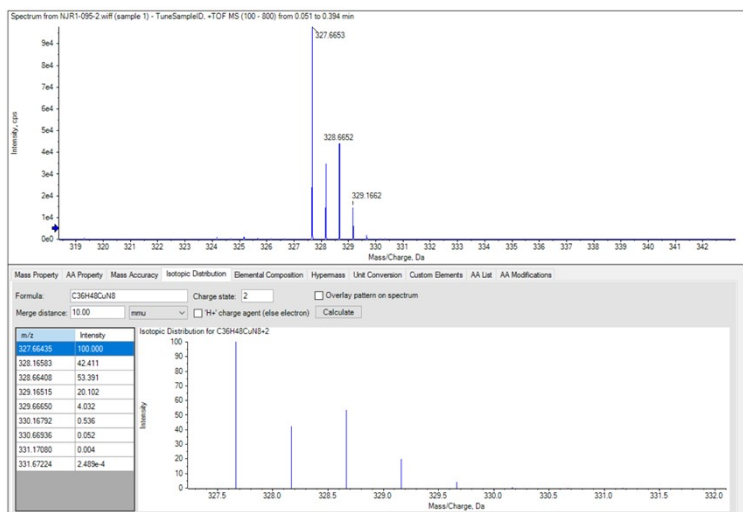


Figure S58 HRMS ES(+) of $[\text{CuL}^{2a}]\text{Cl}_2$

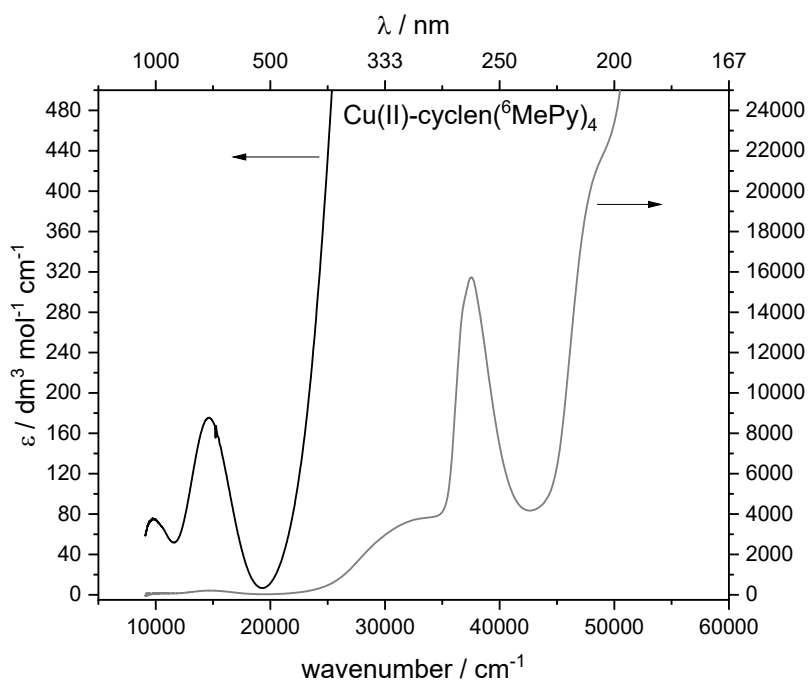


Figure S59 UV-Vis Photoabsorption Spectrum of $[\text{CuL}^{2a}]\text{Cl}_2$ in water (measured at 3 mM and 30 μM).

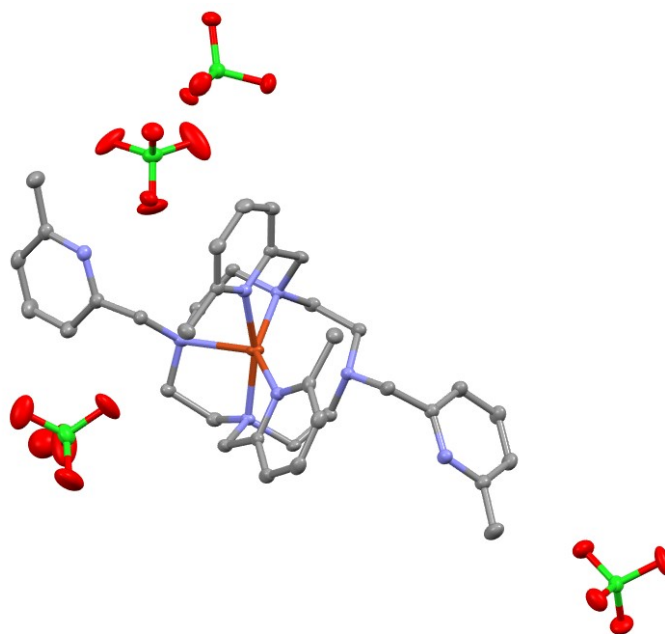
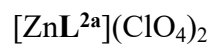


Figure S60. Asymmetric unit of the crystal structure of [CuL^{2a}-H₂](ClO₄)₄, displayed as a thermal ellipsoid plot (50% probability), with H atoms removed for clarity. The asymmetric unit contains the Δ-λλλλ conformational isomer. X-ray crystallography performed at 100 K.



Apr29-2024.1.fid
NJR1-141
Zn-cyclen-6MePy4 perchlorate

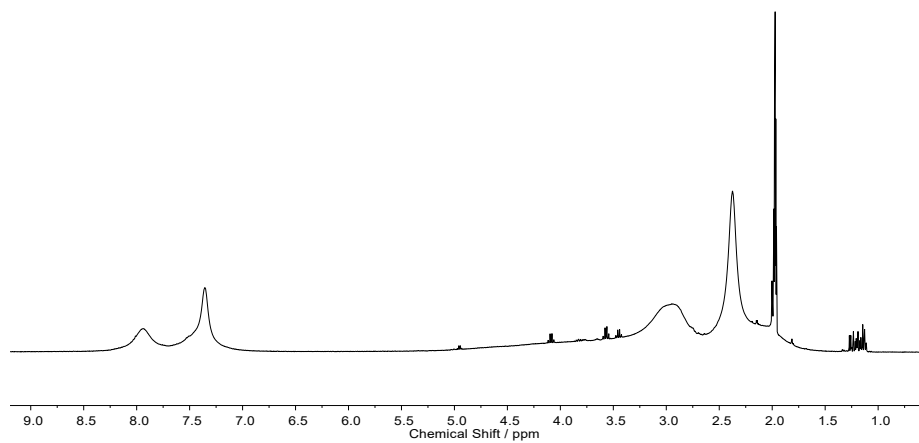


Figure S61 ^1H NMR (400 MHz, CD_3CN , 296 K) of $[\text{ZnL}^{2a}](\text{ClO}_4)_2$

NJR1-141.1.fid
NJR1-141
CD3CN

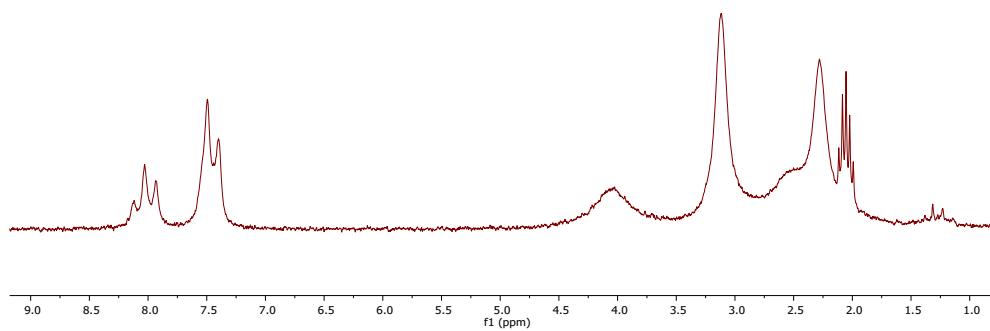


Figure S62 ^1H NMR (80 MHz, CD_3CN , 300 K) of $[\text{ZnL}^{2a}](\text{ClO}_4)_2$

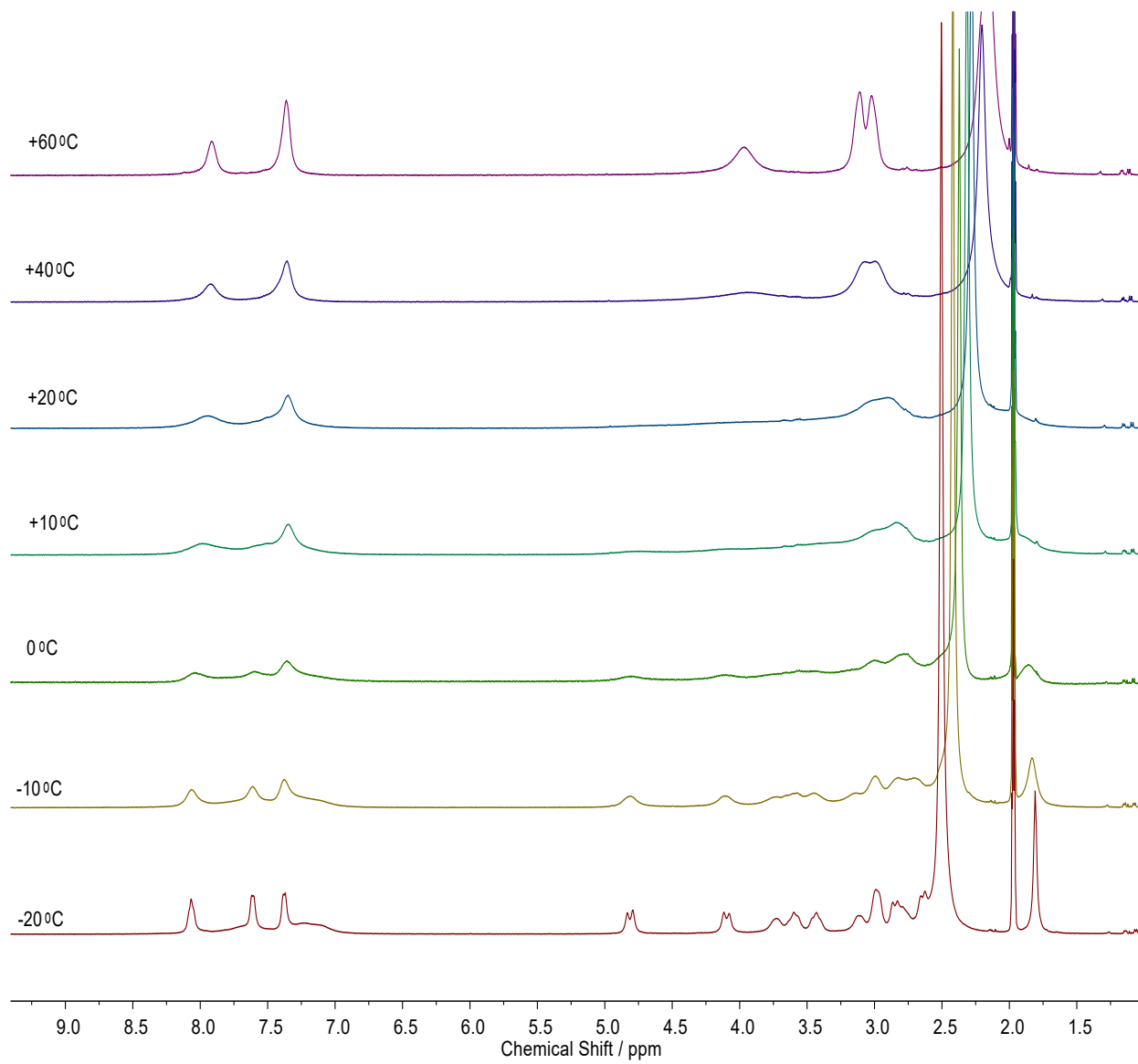


Figure S63 Variable Temperature ¹H NMR (400 MHz, CD₃CN) of [ZnL^{2a}](ClO₄)₂

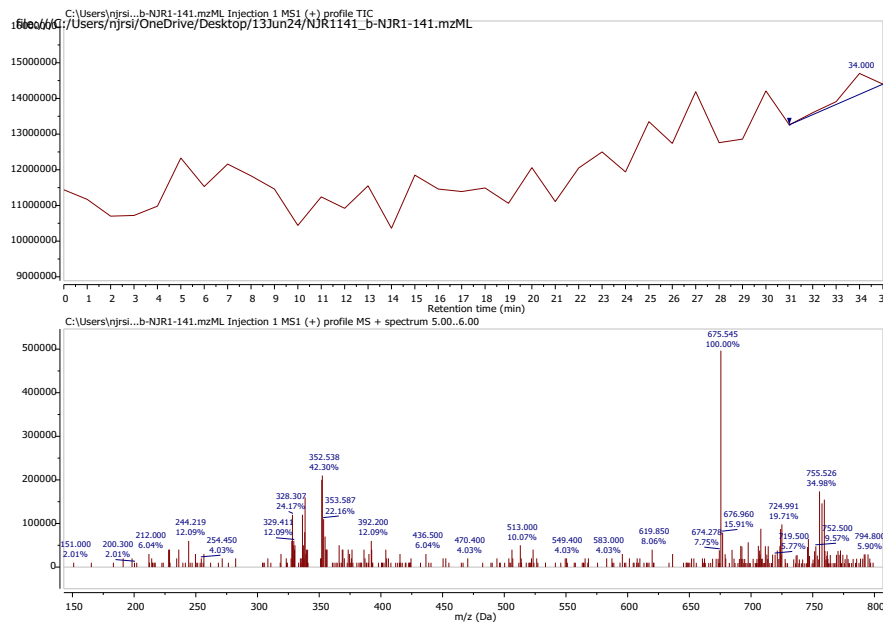


Figure S64 LRMS ES(+) of $[\text{ZnL}^{2a}](\text{ClO}_4)_2$

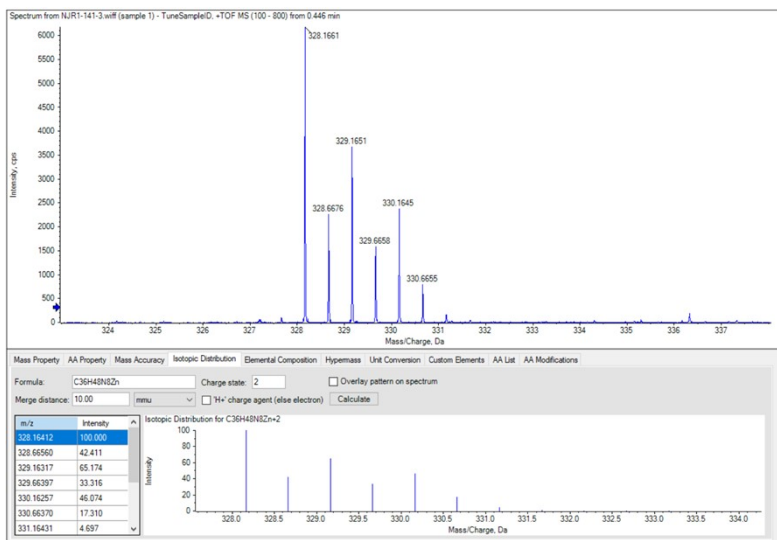


Figure S65 HRMS ES(+) of $[\text{ZnL}^{2a}](\text{ClO}_4)_2$

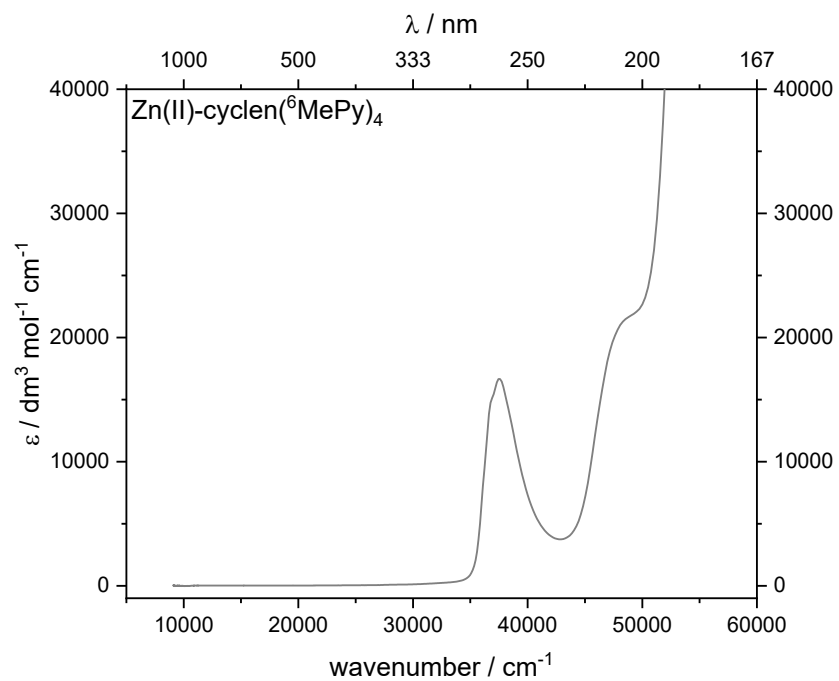


Figure S66 UV-Vis Photoabsorption Spectrum of [ZnL^{2a}](ClO₄)₂ in 0.5% CH₃CN, water (measured at 30 μM).

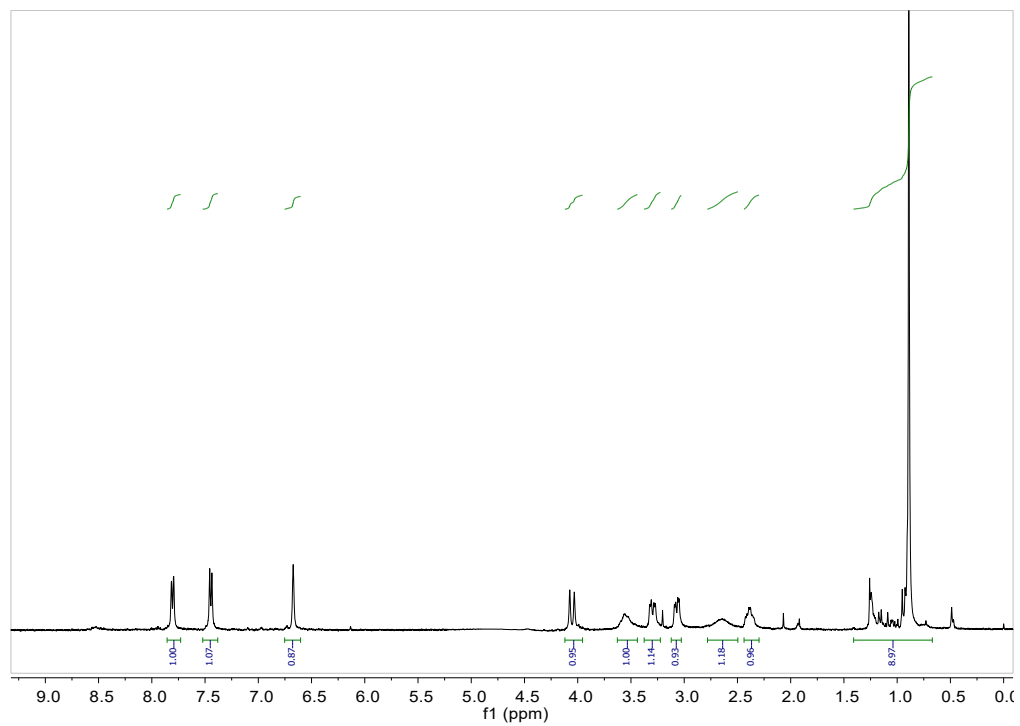


Figure S67 ¹H NMR (400 MHz, D₂O, 296 K, with solvent suppression) of [FeL^{1b}]Cl₂

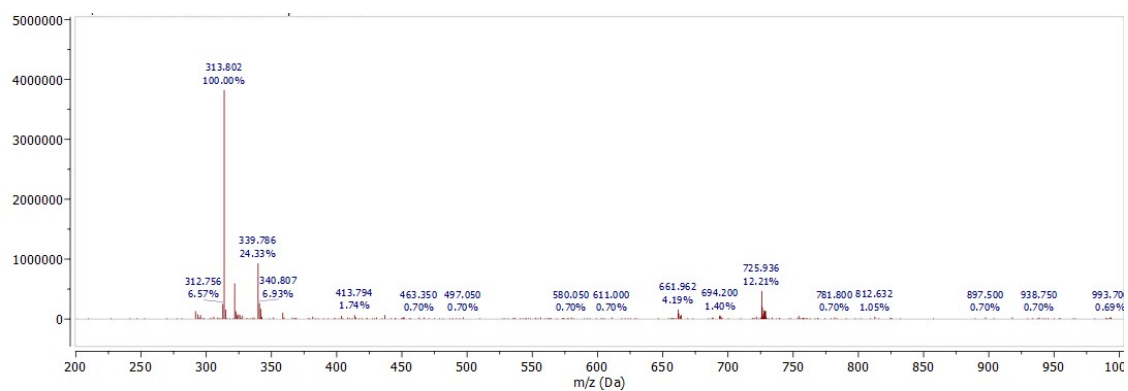


Figure S68 LRMS ES(+) of [FeL^{1b}]Cl₂

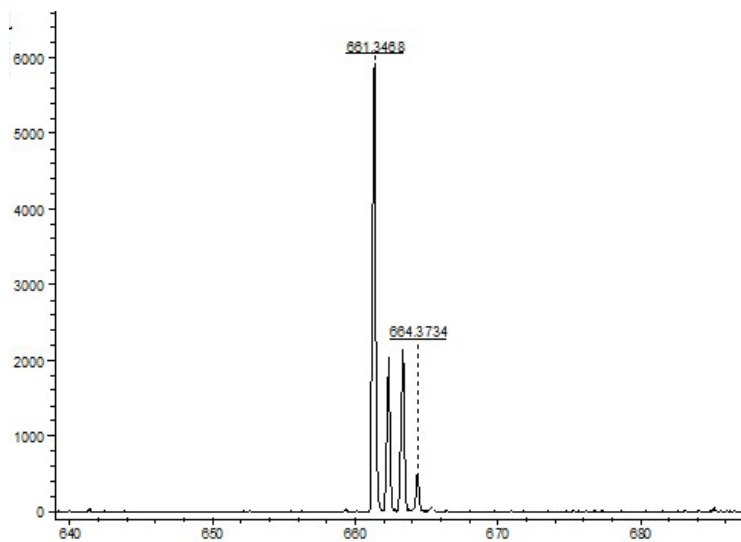


Figure S69 HRMS MALDI-TOF(+) of $[\text{FeL}^{1b}]\text{Cl}_2$

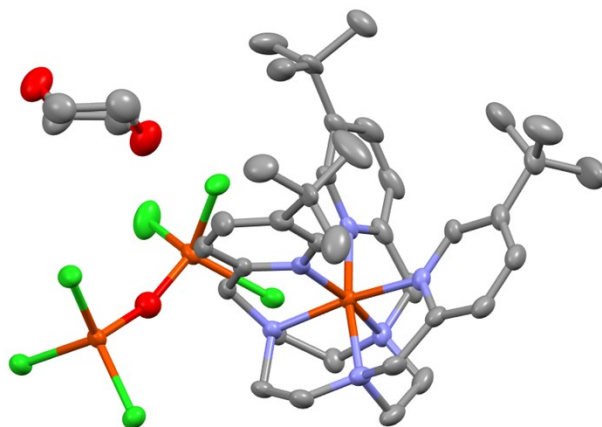


Figure S70 Asymmetric unit of the crystal structure of $[\text{Fe}(\text{II})\text{L}^{1b}][(\text{Fe}(\text{III})\text{Cl}_3)_2\text{-O}]$ with solvent, displayed as a thermal ellipsoid plot (50% probability), with H atoms removed for clarity. The asymmetric unit contains the $\Delta(\lambda\lambda\lambda)$ conformational isomer. X-ray crystallography performed at 100 K.

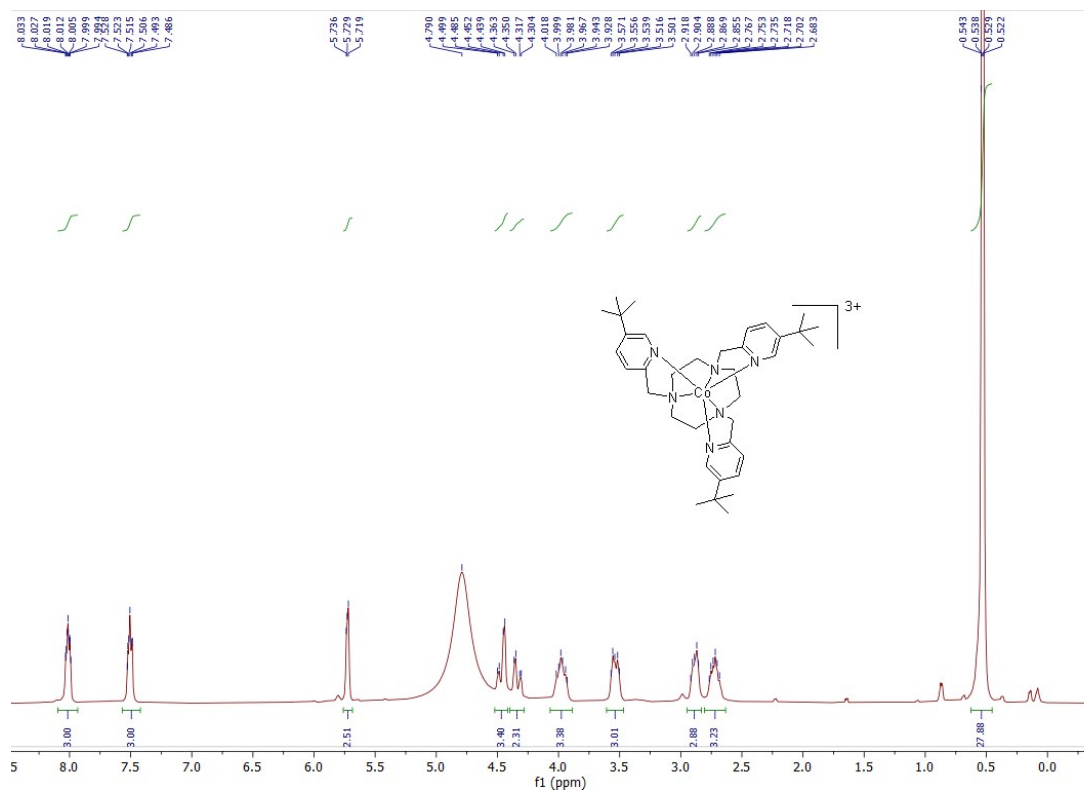


Figure S71 ¹H NMR (400 MHz, D₂O, 296 K) of [CoL^{1b}]Cl₃

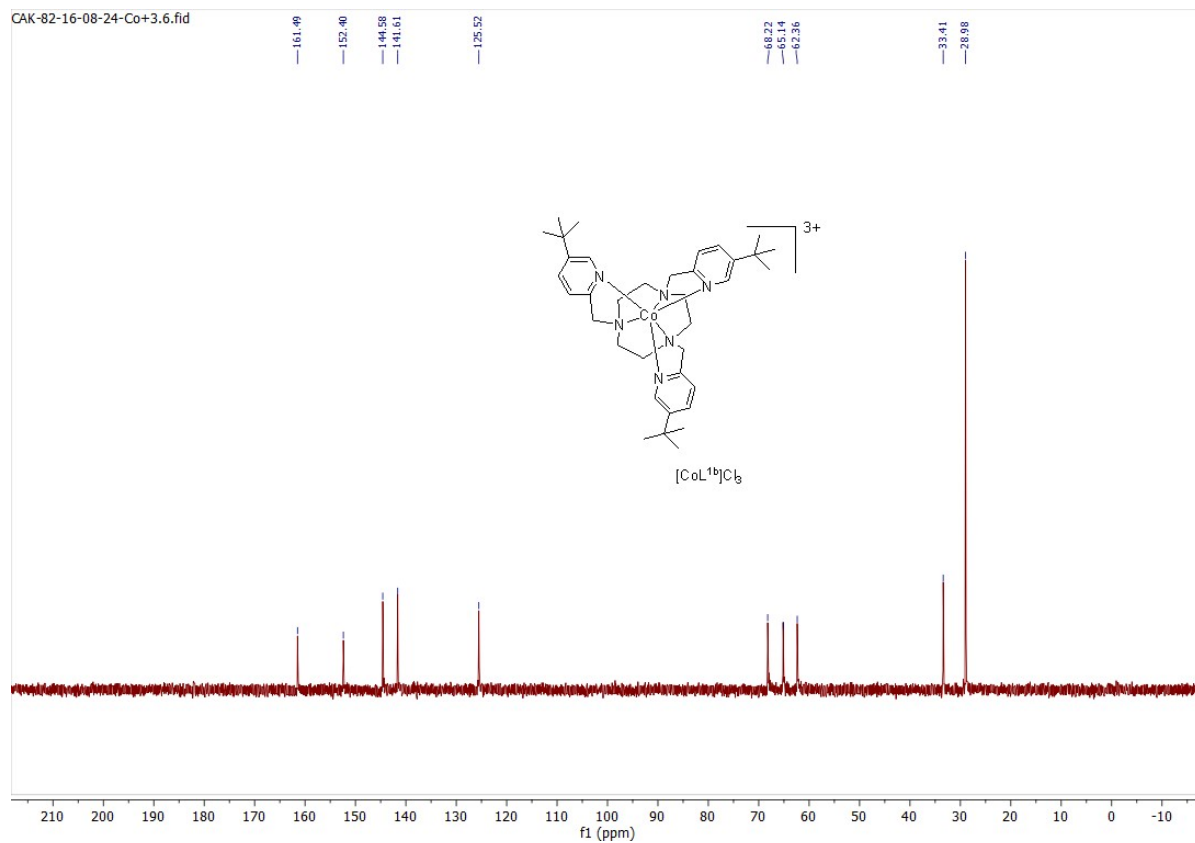


Figure S72 ^{13}C NMR (400 MHz, D_2O , 296 K) of $[\text{CoL}^{1b}]\text{Cl}_3$

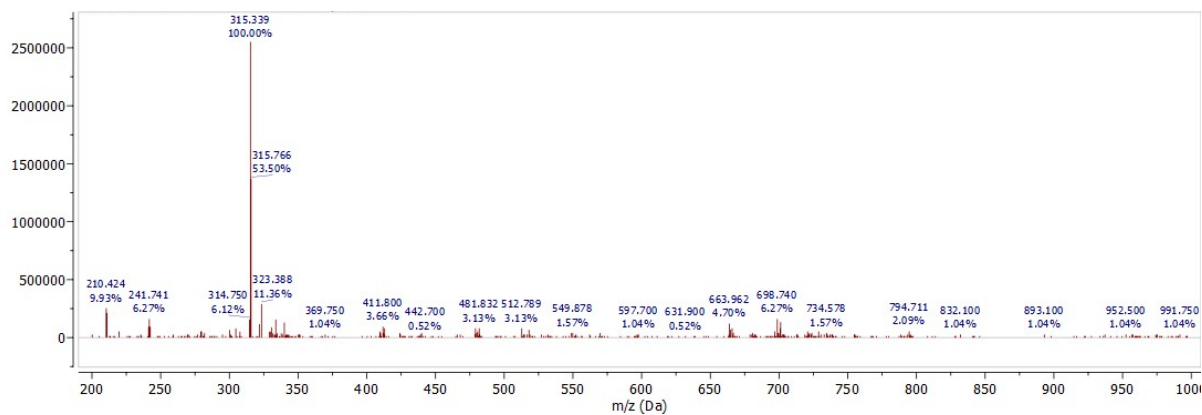


Figure S73 LRMS ES(+) of $[\text{CoL}^{1b}]\text{Cl}_3$

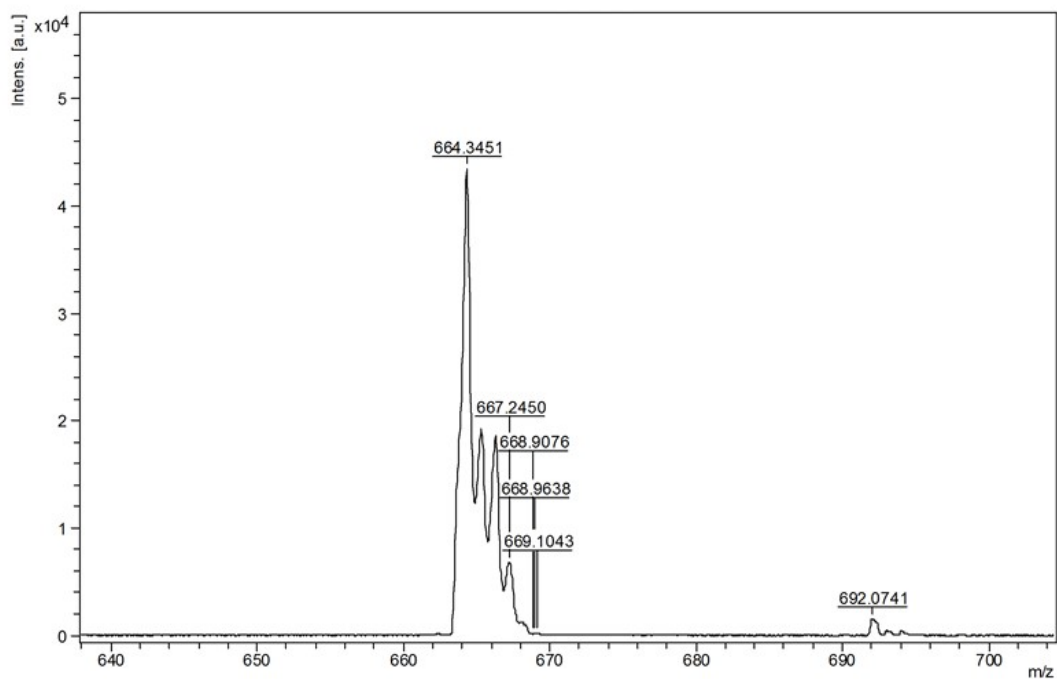


Figure S74 MALDI-TOF HRMS(+) of $[\text{CoL}^{1b}]\text{Cl}_3$

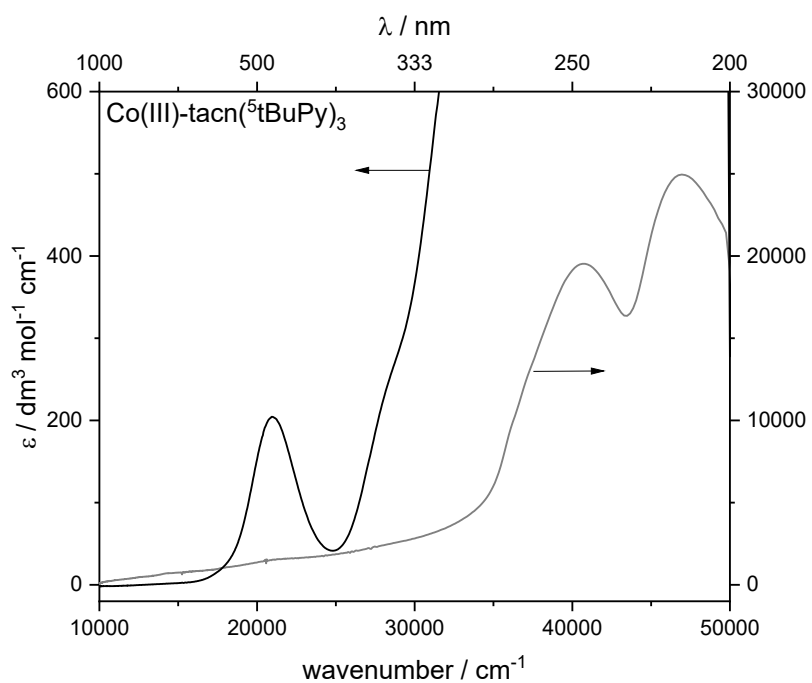


Figure S75 UV-Vis Photoabsorption Spectrum of $[\text{CoL}^{1b}]\text{Cl}_3$ in water (measured at 3 mM and 30 μM).

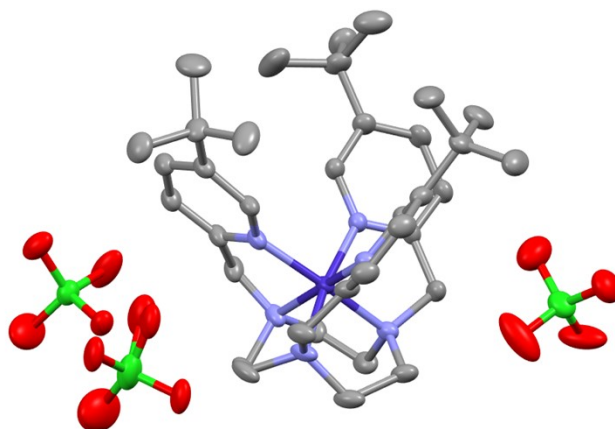


Figure S76. Asymmetric unit of the crystal structure of [Co(III)L^{1b}][(ClO₄)₃], displayed as a thermal ellipsoid plot (50% probability), with H atoms removed for clarity. The asymmetric unit contains the $\Delta(\lambda\lambda\lambda)$ conformational isomer. X-ray crystallography performed at 100 K.

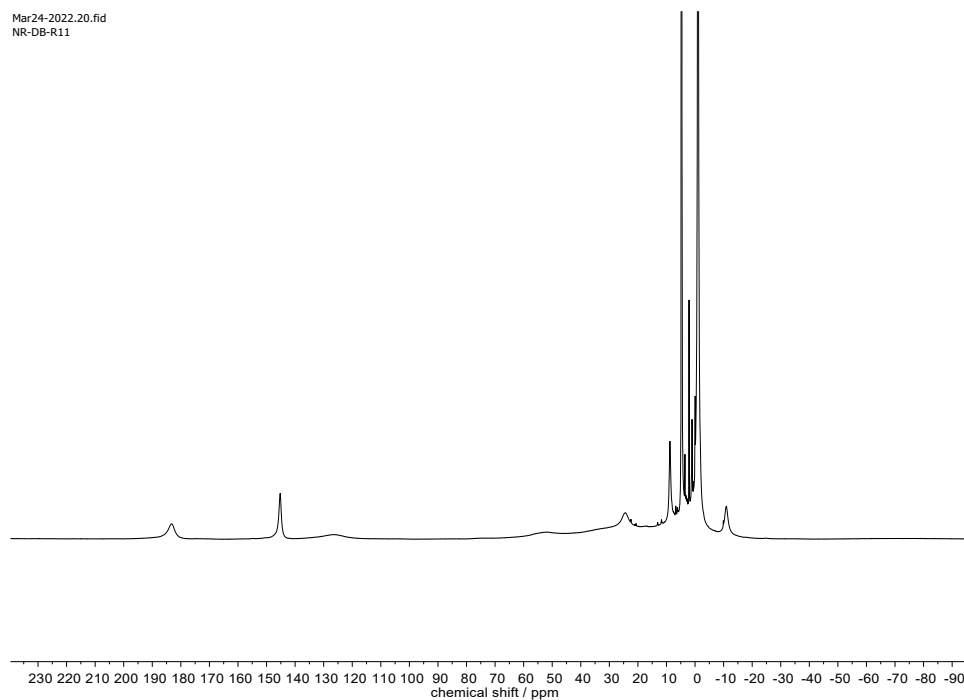
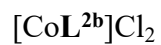


Figure S77 ^1H NMR (500 MHz, D_2O , 296 K) of $[\text{CoL}^{2b}]\text{Cl}_2$.

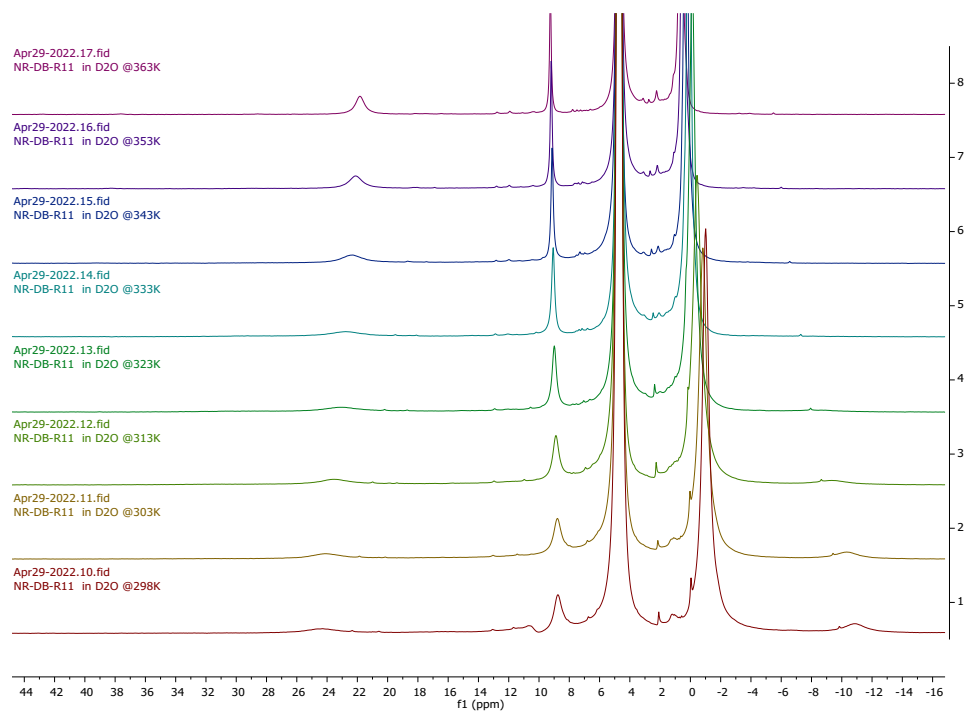


Figure S78 Variable temperature ^1H NMR (500 MHz, D_2O , 296 K) of $[\text{CoL}^{2b}]\text{Cl}_2$.

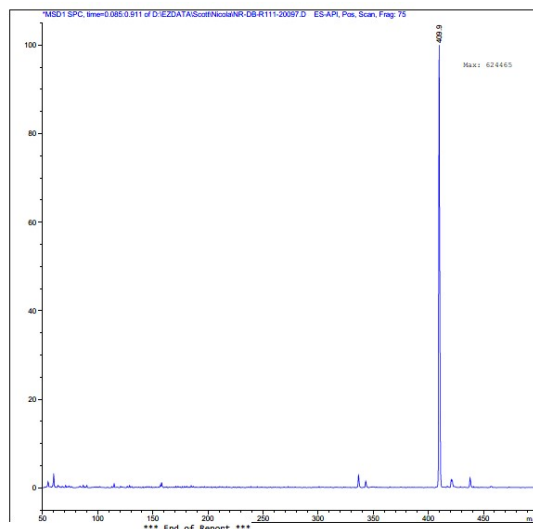


Figure S79 LRMS ES(+) of $[\text{CoL}^{2b}]\text{Cl}_2$.

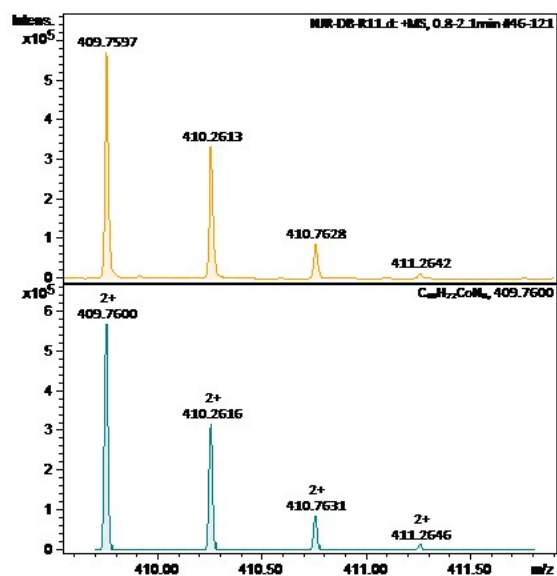


Figure S80 HRMS ES(+) of $[\text{CoL}^{2b}]\text{Cl}_2$, found (top) and predicted (bottom).

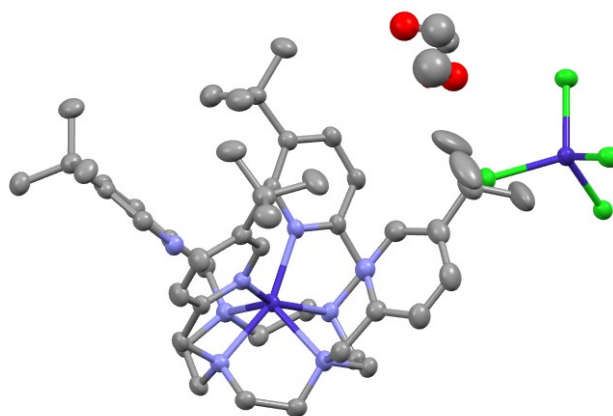


Figure S81. Asymmetric unit of the crystal structure of $[\text{CoL}^{2b}][\text{CoCl}_4]$, displayed as a thermal ellipsoid plot (50% probability), with three disordered solvent molecules. H atoms removed for clarity. The asymmetric unit contains the Δ - $\delta\delta\delta\delta$ conformational isomer. X-ray crystallography performed at 100 K.

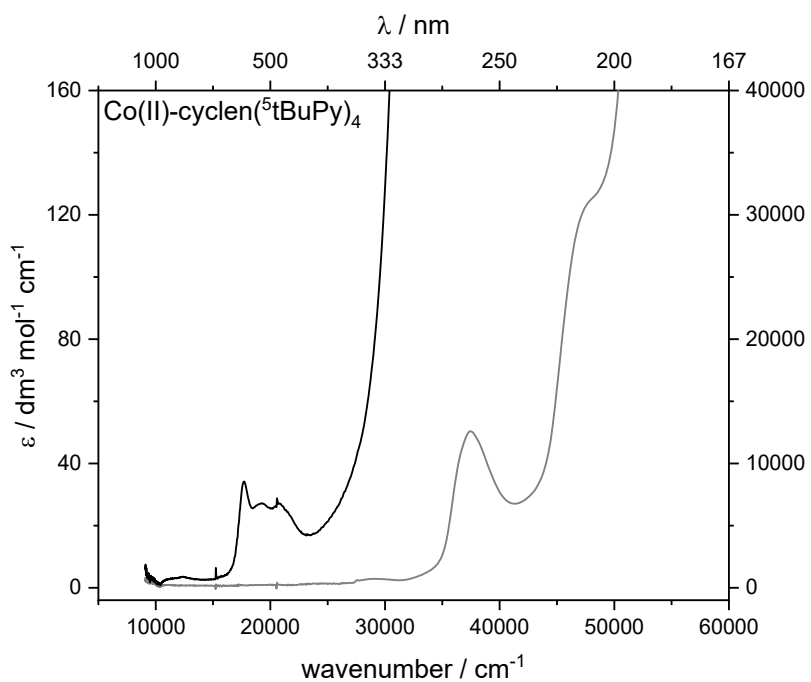


Figure S82 UV-Vis Photoabsorption Spectrum of $[\text{CoL}^{2b}]\text{Cl}_2$ in water (measured at 3 mM and 30 μM).

4. ^1H NMR spectra of $[\text{ML}^{\text{1a}}]^{2+}$ and $[\text{ML}^{\text{2a}}]^{2+}$ complexes at 9.4 T

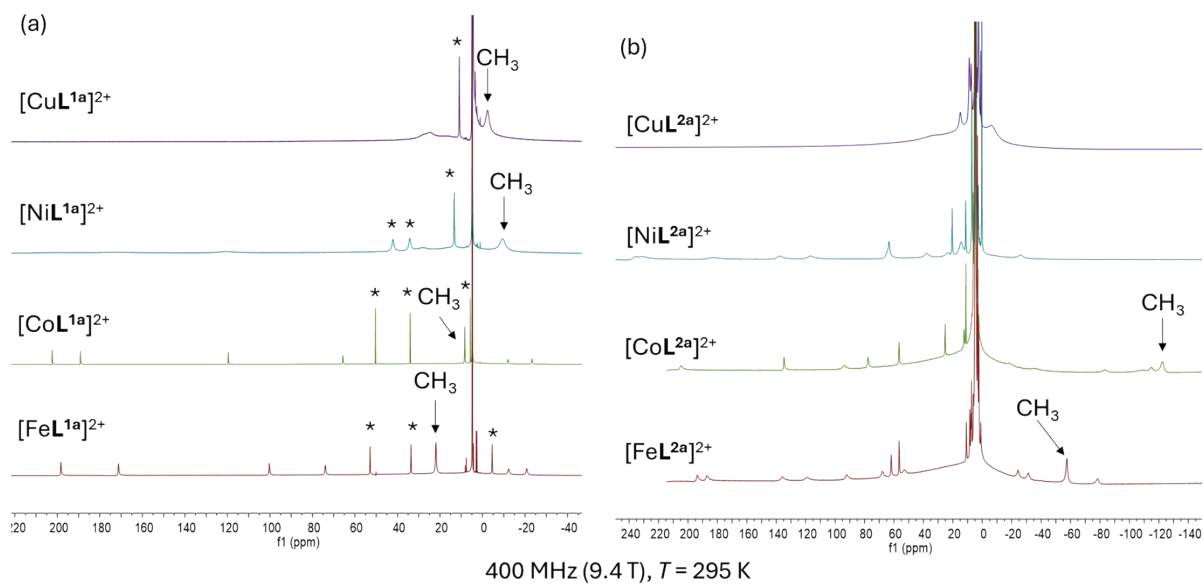


Figure S83 ^1H NMR spectra of $[\text{ML}^{\text{1a}}]^{2+}$ and $[\text{ML}^{\text{2a}}]^{2+}$ ($M = \text{Fe(II)}$, Co(II) , Ni(II) , Cu(II)) at 400 MHz (9.4 T, 295 K) in D_2O

5. Fitting Field-dependent Proton Relaxation Data

Field-dependent R_1 rates of $[\text{FeL}^{1a}]^{2+}$, $[\text{CoL}^{1a}]^{2+}$, $[\text{FeL}^{2a}]^{2+}$, $[\text{CoL}^{2a}]^{2+}$, and $[\text{NiL}^{1a}]^{2+}$ were measured in the 1.4-16.4 T range.

Table S1. Measured ^1H relaxation rates, R_1 , of $[\text{ML}^{1a}]\text{Cl}_2$ and $[\text{ML}^{2a}]\text{Cl}_2$ at variable magnetic fields

Complex	δ / ppm^a	proton	R_1 / Hz^a				
			1.4 T (299 K)	1.9 T (300 K)	9.4 T (296 K)	14.1 T (295 K)	16.4 T (298 K)
$[\text{FeL}^{1a}]^{2+}$	+53	Py-H ⁵	24±2	26±1	34±2	46±2	47±1
$[\text{CoL}^{1a}]^{2+}$	+50	Py-H ⁵	19±2	18±1	18±1	25±1	31±1
$[\text{NiL}^{1a}]^{2+}$	+34	Py-H ^{3/5}	420±40	356±14	477±4	453±16	450±11
$[\text{FeL}^{2a}]^{2+}$	-57	Py-CH ₃	760±180	730±70	875±3	935±5	950±25
$[\text{CoL}^{2a}]^{2+}$	+134	?	^b	525±50	396±2	394±4	405±5

^ameasured at 295-300 K. ^b R_1 not measurable as broad signal and fast relaxation.

Intramolecular nuclear relaxation rates are enhanced by paramagnetic metal centres via both contact and pseudocontact mechanisms, but they are often modelled using Bloch-Redfield-Wangness theory, as shown in Equations 1 and 2, which treat the through-space rotational and conformational modulation of the electron-nuclear interaction only, models the spins as point dipoles, and assumes that the magnetic susceptibilities and the molecular reorientations are isotropic.

$$R_1 = \frac{2}{15} \left(\frac{\mu_0}{4\pi} \right)^2 \frac{\gamma_H^2 \mu_{eff}^2}{r^6} \left(\frac{7\tau_c}{1 + \omega_e^2 \tau_c^2} + \frac{3\tau_c}{1 + \omega_H^2 \tau_c^2} \right) + \frac{2}{5} \left(\frac{\mu_0}{4\pi} \right)^2 \frac{\omega_H^2 \mu_{eff}^4}{(3k_B T)^2 r^6} \left(\frac{3\tau_r}{1 + \omega_H^2 \tau_r^2} \right)$$

Equation 1

$$R_2 = \frac{1}{15} \left(\frac{\mu_0}{4\pi} \right)^2 \frac{\gamma_H^2 \mu_{eff}^2}{r^6} \left(4\tau_c + \frac{13\tau_c}{1 + \omega_e^2 \tau_c^2} + \frac{3\tau_c}{1 + \omega_H^2 \tau_c^2} \right) + \frac{1}{5} \left(\frac{\mu_0}{4\pi} \right)^2 \frac{\omega_H^2 \mu_{eff}^4}{(3k_B T)^2 r^6} \left(4\tau_r + \frac{3\tau_r}{1 + \omega_H^2 \tau_r^2} \right)$$

Equation 2

Where μ_0 is the permeability of a vacuum, γ_H is the gyromagnetic ratio of a proton, μ_{eff} is the effective magnetic moment of the paramagnetic metal complex, r is the electron-nucleus intramolecular distance, τ_r is the rotational correlation time of the molecule, T_{1e} is the electronic relaxation time, τ_c is the correlation time ($\tau_c^{-1} = \tau_r^{-1} + T_{1e}^{-1}$), ω_e is the Larmor frequency of an electron, ω_H is the Larmor frequency of a proton, k_B is the Boltzmann constant, T is the absolute temperature.

These equations (1 and 2) each comprise two terms; the former dipolar term, which describes relaxation mechanism due to the modulation of the dipole coupling with the electron spin on the time-scale of electronic relaxation, and the latter Curie term, describing the dipole-dipole interaction between the nucleus and the *averaged* electronic magnetic moment, that correlated with the slower molecular rotation time.

The measured proton relaxation rates (R_1) were fitted using a modified Matlab code originally written by Prof. Ilya Kuprov (Weizmann Institute of Science). The algorithm uses Equation 1 to fit the R_1 data using the Matlab internal Levenberg Marquardt minimization of the non-linear squares error function, in order to estimate T_{1e} , similar to previous analyses with lanthanide complexes.^{20, 23} The field-dependent R_1 data were fitted using fixed experimental values of μ_{eff} (dashed lines), giving values of r , τ_r , and T_{1e} . r and τ_r were compared to expected experimental values.

Error analysis was performed by varying the temperature and the R_1 values by the stated errors and evaluating the variation in the fitted values of r , τ_r , and T_{1e} :

CoL2a					
4.1960	447.2281	1.1569	298 K	525 396 394 405	
4.2031	453.5119	1.1705	295 K		%change temp
4.1913	443.0928	1.1480	300 K		%change temp
4.1610	435.5154	0.9654	298 K	475 396 394 405	%change 80 MHz
4.2410	468.3309	1.4110	298 K	575 396 394 405	%change 80 MHz
4.1927	470.5164	1.148	298 K	525 396 390 400	%change 14.1 and 16.4 lower
4.1982	425.5413	1.1631	298 K	525 396 398 410	%change 14.1 and 16.4 upper
4.1998	430.2487	1.1660	298 K	525 396 394 410	%change 16.4 T lower
4.1706	439.2998	0.9810	298 K	475 392 390 400	all lower limit
4.2369	452.8199	1.4013	298 K	575 398 398 410	all upper limit

$T_{1e} = 1.2(2)$
 $r = 4.20(5)$
 $\tau_r = 450 (25)$

FeL2a					
3.5957	374.7661	0.5784	298 K	760 730 875 935 950	
3.6032	377.7035	0.5857	295 K		%change Temp
3.5908	372.8440	0.5737	300 K		%change Temp
3.5389	440.5066	0.4252	298 K	580 660 875 935 950	%change 60 and 80 MHz Lower
3.6332	344.2651	0.7351	298 K	940 800 875 935 950	%change 60 and 80 MHz Upper
3.5935	404.5277	0.5746	298 K	760 730 875 930 925	%change 14.1 and 16.4 lower
3.5960	347.2819	0.5802	298 K	760 730 875 940 975	%change 14.1 and 16.4 upper

$T_{1e} = 0.59(16)$
 $r = 3.6 (1)$
 $\tau_r = 380 (60)$

CoL1a					
5.6481	76.3065	0.2667	298 K	19 18 18 25 31	
5.6802	78.7295	0.2763	295 K		%change Temp
5.6257	74.6074	0.2601	300 K		%change Temp
5.8208	98.2636	0.3492	298 K	21 19 18 25 31	% 60/80 Upper
4.2321	10.4422	0.0430	298 K	17 17 18 25 31	%60/80 Lower - No sensible minimisation.
5.4522	59.7619	0.2131	298 K	19 18 18 26 32	%14.2/16.4 Upper
5.7680	86.8487	0.3058	298 K	19 18 18 24 30	%14.2/16.4 Lower

$T_{1e} = 0.27(0.08)$
 $r = 5.6(0.2)$
 $\tau_r = 80 (20)$

FeL1a					
5.6783	199.0601	0.3429	298 K	24 26 34 46 47	
5.6940	200.0558	0.3486	295 K		
5.6680	198.4212	0.3392	300 K		
5.6735	216.2106	0.3191	298 K	22 25 34 46 47	
5.6772	182.7676	0.3646	298 K	26 27 34 46 47	

5.7172 206.4981 0.3584
5.6406 193.1058 0.3282

298 K 24 26 34 44 46
298 K 24 26 34 48 48

T1e = 0.34(0.02)
r = 5.7(0.1)
tau_r = 200 (20)

Errors for NiL1a

5.3330 279.3507 39.3651
5.3315 279.4532 39.2753
5.3340 279.2845 39.4235
5.3794 275.6491 40.7430
5.2569 288.6939 36.4865
5.3603 293.2814 39.9585
5.3102 269.8885 38.9255

298 K 420 356 477 453 450
295 K
300 K
298 K 380 344 477 453 450
298 K 460 372 477 453 450
298 K 420 356 477 437 439
298 K 420 356 477 469 461

T1e = 39(3)
r = 5.3(0.1)
tau_r = 280(15)

6. Phantom Imaging Experiments

Phantom imaging was performed using a 30 mm ^1H imaging coil (Bruker, Germany) at 9.4 T, 298 K.

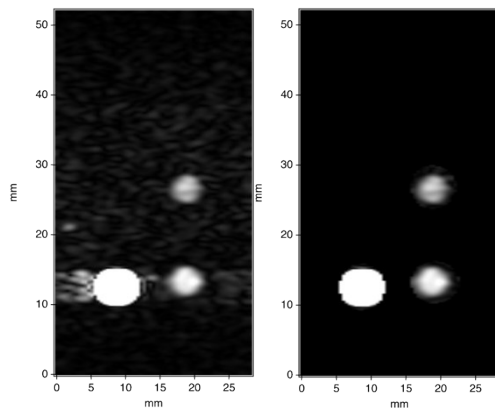


Figure S84 Non-slice selective 2D gradient echo MRI of two 5 mm tubes (cross-section) containing water (left) and 10 mM $[\text{FeL}^{2a}]^{2+}$ dissolved in D_2O , 9.4 T. TR=40 ms, TE=1.48 ms, NS=512, SW=249 ppm (100 kHz) matrix size = 256 \times 32. Raw data (left) and processed data (right) using ROI mapping to remove noise. Image acquired in 12 min.